INSTITUTE OF PHYSICS PUBLISHING WAVES IN RANDOM MEDIA

Waves Random Media **11** (2001) 119–147 www.iop.org/Journals/wr PII: S0959-7174(01)18444-2

Bistatic scattering coefficient from one- and two-dimensional random surfaces using the stationary phase and scalar approximation with shadowing effect: comparisons with experiments and application to the sea surface

C Bourlier[1], **G Berginc**[2] **and J Saillard**[1]

[1] IRCCyN, UMR no 6597 CNRS, Division SETRA, Ecole Polytechnique de l'Université de Nantes, IRESTE, Rue Christian Pauc, La Chantrerie, BP 60601, 50609 Nantes Cedex 3, France
[2] DS/DFO, Thales Optronique, Rue Guynemer, BP 55, 78283 Guyancourt Cedex, France

E-mail: cbourlie@ireste.fr

Received 30 October 2000, in final form 30 January 2001

Abstract

In this paper, the bistatic scattering coefficient from one- and two-dimensional random surfaces using the stationary phase method and scalar approximation with shadowing effect is investigated. Both of these approaches use the Kirchhoff integral. With the stationary phase, the bistatic cross section is formulated in terms of the surface height joint characteristic function where the shadowing effect is investigated. In the case of the scalar approximation, the scattering function is computed from the previous characteristic function and in terms of expected values for the integrations over the slopes, where the shadowing effect is analysed analytically. Both of these formulations are compared with experimental data obtained from a Gaussian one-dimensional randomly rough perfectly-conducting surface. With the stationary-phase method, the results are applied to a two-dimensional sea surface.

1. Introduction

The problem of electromagnetic wave scattering from a randomly rough surface has been widely studied because of its relevance in the fields of telecommunications and remote sensing. Among the many surface-scattering theories, the Kirchhoff approximation is one of the most widely used. We can also quote the integral equation based on the Monte Carlo technique (Thorsos *et al* [6, 7]), the small-slope approximation (SSA) developed by Voronovich [5] and the perturbation approximation (Thorsos and Broschat [8–10] and Chevalier and Berginc [11]). The Kirchhoff approximation or physical optics, which is the most widely used (Olgivy [3], Ulaby *et al* [1,2] and Beckmann and Spizzichino [4]) is investigated in this paper. The Kirchhoff approach uses the tangent plane approximation, which is valid when both the average radius

 © 2001 IOP Publishing Ltd Printed in the UK

of the curvature and the horizontal roughness (correlation length for a stochastic process) are large relative to the wavelength [1]. However, as it stands, the expression of the scattered field is a complicated function of the surface height and its partial derivatives [12] (Bourlier *et al*), which involves there being no analytic solution without additional simplifying assumptions. The stationary phase approximation can be used with a homogeneous random surface (the rough surface spectral density functions are independent of position), and assumes that the resulting scattered field expression contains only contributions from specular points on the surface. Therefore, the scattering coefficient can be expressed analytically in terms of the surface height joint characteristic function (the Fourier transform of the surface height joint probability density function, PDF). The scalar approximation [1] is obtained from expanding the Kirchhoff integral over the slopes and keeping only the slope terms of first order. In the literature, the fact that the surface is assumed to be isotropic involving the surface height autocorrelation function being independent of the azimuthal direction. If the shadowing function is ignored and if we assume a Gaussian PDF, then the surface height joint characteristic function is also Gaussian. From the Kirchhoff integral with a correlated height and slope Gaussian process, Bourlier *et al* [12] studied the shadowing effect on the backscattering coefficient (monostatic configuration) for perfectly-conducting one- and two-dimensional rough surfaces. They showed that the shadowing effect may be small in the monostatic case.

In this paper, the monostatic and bistatic shadowing effects [13–16] on the scattering coefficient for one- and two-dielectric rough sea surfaces are investigated by applying the stationary phase and scalar approximations [1]. Sancer [17] studied the influence of the shadowing effect on the scattering coefficient obtained from the Kirchhoff theory. He showed that under the geometrical optics approximation, the shadowing function is statistically independent of the unshadowed scattering coefficient, which involves the characteristic function being statistically independent of the shadowing function. Strictly speaking, it is exact only if the shadowing function is assumed to be independent of the surface height. In practice, this is not the case since the function really does depend on the surface height.

The plan of this work is as follows. In section 2, the stationary phase method and the scalar approximation are described in terms of the surface height joint characteristic function and expected values by including the field polarization. In section 3, the surface height joint characteristic function and the expected values with the monostatic and bistatic Smith shadowing functions are performed, for one- and two-dimensional surfaces. From the results of section 3, section 4 compares the incoherent unshadowed and shadowed scattering coefficients with experimental data [18] for different locations of the receiver and transmitter. From the stationary phase method, the scattering coefficient is also applied to a Gaussian two-dimensional sea surface. The height autocorrelation function is given by [19] calculated from the spectrum established by Elfouhaily *et al* [20]

2. Scattered field from the stationary phase and scalar approximation

This section presents the scattered field from a dielectric rough surface by using the stationary phase and scalar approximation. Both of these methods are studied in order to compare them with experimental data.

The scattering coefficient σ_{pq} for an extended target can be written as [1]

$$\sigma_{pq} = \frac{4\pi R_0^2 \langle |E_{pq}|^2 \rangle}{A_0 |E_0|^2} \tag{1}$$

where A_0 is the illuminated area, the symbol $\langle \cdots \rangle$ denotes the ensemble average and R_0 is the range from the centre of the illuminated area S' to the point of observation (figure 1).

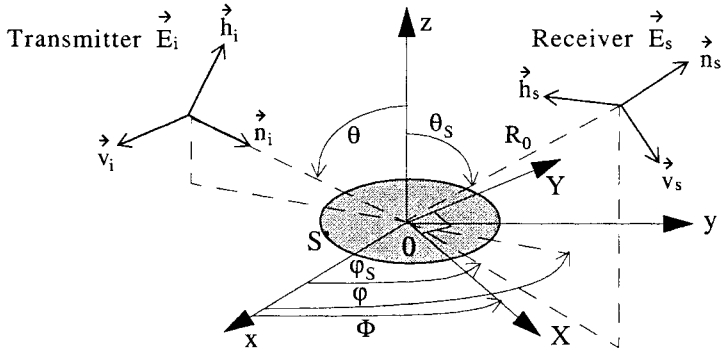

Figure 1. Geometry of the surface-scattering problem in the FSA convention.

E_0 denotes the magnitude of the incident field, and E_{pq} is the scattered field from the rough surface. The horizontal or vertical polarizations are denoted by $\{p, q\}$.

2.1. The stationary phase approximation

The stationary phase method is commonly used to evaluate the scattered field over a rough surface. This approach is valid when both the radius of curvature at each point of the surface and the correlation length are larger than the incident electromagnetic wavelength [1]. This is also discussed in detail in [21, 22]. The stationary phase method assumes that the major contributions of the scattered field from the rough surface come from regions around the specular direction. This assumption means that the normal of the surface is independent of the surface slopes. The scattered field E_{pq}^{SP} can be expressed (in the Fraunhofer region) as [1]

$$E_{pq}^{SP} = K I_{SP} E_0 U_{pq}^{SP} \tag{2}$$

with

$$K = \frac{-\mathrm{j}k \exp(-\mathrm{j}k R_0)}{4\pi R_0} \qquad I_{SP} = \iint \exp[\mathrm{j}k(\vec{n}_s - \vec{n}_i) \cdot \vec{r}'] \, \mathrm{d}S' \tag{2a}$$

where k is the wavenumber in the medium where the field is evaluated, R_0 ranges from the centre of the illuminated area S' to the point of observation (see figure 1), $\{\vec{n}_i, \vec{n}_s\}$ are the unit vectors in the scattered and incident directions, respectively, defined in spherical coordinates as

$$\begin{aligned} \vec{n}_i &= \sin\theta \cos\varphi \vec{x} + \sin\theta \sin\varphi \vec{y} - \cos\theta \vec{z} \\ \vec{n}_s &= \sin\theta_s \cos\varphi_s \vec{x} + \sin\theta_s \sin\varphi_s \vec{y} + \cos\theta_s \vec{z} \end{aligned} \tag{3}$$

where $(\vec{x}, \vec{y}, \vec{z})$ are unit vectors in Cartesian coordinates. $\vec{r}' = x'\vec{x} + y'\vec{y} + z'(x', y')\vec{z}$ is the vector indicating the location of the surface point according to the centre of the illuminated area. In (2), U_{pq}^{SP} denotes a polarization term where $\{p, q\}$ denote $\{h_i, v_i, h_s, v_s\}$ (horizontal

or vertical polarization for the incident and scattered fields), and given by [1]

$$\begin{aligned}
U^{SP}_{h_s h_i} &= \frac{r_1 R_V + r_2 R_H}{D} \qquad & r_1 &= (\vec{h}_s \cdot \vec{n}_i)(\vec{h}_i \cdot \vec{n}_s) \\
U^{SP}_{v_s h_i} &= \frac{r_3 R_V - r_4 R_H}{D} \qquad & r_2 &= (\vec{v}_s \cdot \vec{n}_i)(\vec{v}_i \cdot \vec{n}_s) \\
U^{SP}_{v_s v_i} &= \frac{r_2 R_V + r_1 R_H}{D} \qquad & r_3 &= (\vec{v}_s \cdot \vec{n}_i)(\vec{h}_i \cdot \vec{n}_s) \\
U^{SP}_{h_s v_i} &= \frac{r_4 R_V - r_3 R_H}{D} \qquad & r_4 &= (\vec{h}_s \cdot \vec{n}_i)(\vec{v}_i \cdot \vec{n}_s) \\
D &= \frac{k q_z [(\vec{h}_s \cdot \vec{n}_i)^2 + (\vec{v}_s \cdot \vec{n}_i)^2]}{|q_z| q}
\end{aligned} \tag{4}$$

where $\{R_V, R_H\}$ are the Fresnel coefficients in vertical V and horizontal H polarizations evaluated with an incidence angle θ_1 equal to $\theta_1 = a\cos[q|q_z|/(2kq_z)]$. The vectors $\{\vec{h}_i, \vec{v}_i, \vec{h}_s, \vec{v}_s\}$ are defined in the forward scattering alignment (FSA) convention [1, 2] as (see figure 1)

$$\begin{aligned}
\vec{h}_i &= -\sin\varphi\vec{x} + \cos\varphi\vec{y} \\
\vec{v}_i &= \vec{h}_i \wedge \vec{n}_i = -\cos\theta\cos\varphi\vec{x} - \cos\theta\sin\varphi\vec{y} - \sin\theta\vec{z}
\end{aligned} \tag{4a}$$

$$\begin{aligned}
\vec{h}_s &= -\sin\varphi_s\vec{x} + \cos\varphi_s\vec{y} \\
\vec{v}_s &= \vec{h}_s \wedge \vec{n}_s = \cos\theta_s\cos\varphi_s\vec{x} + \cos\theta_s\sin\varphi_s\vec{y} - \sin\theta_s\vec{z}.
\end{aligned} \tag{4b}$$

The terms $\{q, q_z\}$ are obtained from the phase term of I_{SP} integrand

$$k(\vec{n}_s - \vec{n}_i) \cdot \vec{r}' = q_x x' + q_y y' + q_z z'. \tag{5}$$

Using (3) we have

$$\begin{aligned}
q_x &= k(\sin\theta_s\cos\varphi_s - \sin\theta\cos\varphi) \\
q_y &= k(\sin\theta_s\sin\varphi_s - \sin\theta\sin\varphi) \\
q_z &= k(\cos\theta_s + \cos\theta).
\end{aligned} \tag{5a}$$

Substituting (2) into (1), the scattering coefficient σ^{SP}_{pq} is given by

$$\sigma^{SP}_{pq} = \frac{|kU^{SP}_{pq}|^2}{4\pi A_0}\langle |I_{SP}|^2 \rangle \tag{6}$$

with $\langle |I_{SP}|^2 \rangle$ expressed in the rectangular coordinates [1] as

$$\langle |I_{SP}|^2 \rangle = \frac{q^2}{q_z^2}\iiiint \exp\{\mathrm{j}[q_x(x' - x'') + q_y(y' - y'')]\}\langle \exp[\mathrm{j}q_z(z' - z'')]\rangle \,\mathrm{d}x'\,\mathrm{d}y'\,\mathrm{d}x''\,\mathrm{d}y''. \tag{6a}$$

For a homogenous surface (a stationary process), the term $\langle \cdots \rangle$ depends only on the difference variables $u = x' - x''$, $v = y' - y''$. Assuming that the size of the illuminated surface is $2L \times 2L$, equation (6*a*) can be written as [1]

$$\langle |I_{SP}|^2 \rangle = \frac{q^2}{q_z^2}\int_{-2L}^{2L}\int_{-2L}^{2L}(2L - |u|)(2L - |v|)\exp(\mathrm{j}q_x u + \mathrm{j}q_y v)\chi_1(u, v)\,\mathrm{d}u\,\mathrm{d}v \tag{7}$$

where $\chi_1(u, v)$ is the surface height joint characteristic function given by

$$\chi_1(u, v) = FT[p(z', z'')] = \int_{-\infty}^{\infty}\int_{-\infty}^{\infty} \exp[\mathrm{j}q_z(z' - z'')]p(z', z'')\,\mathrm{d}z'\,\mathrm{d}z'' \quad (8)$$

where the symbol FT is the Fourier transform. $p(z', z'')$ denotes the surface height joint probability density (PDF), which depends on the surface height autocorrelation function $R_0(u, v)$ expressed in Cartesian coordinates $\{u, v\}$. For a Gaussian PDF with zero mean, height variance ω^2, normalized surface height autocorrelation function $f_0 = R_0/\omega^2$, and when the shadowing function is not taken into account, we obtain

$$\chi_1(u, v) = \exp\{-q_z^2\omega^2[1 - f_0(u, v)]\}. \quad (9)$$

In conclusion, the scattering coefficient (6) under the stationary phase approximation depends on two main parameters: U_{pq}^{SP} (4) characterizing the polarization as functions of the Fresnel coefficients and the problem geometry and $\langle|I_{SP}|^2\rangle$ (7) which defines the surface random behaviour as a function of the surface height joint characteristic function $\chi_1(u, v)$. For a Gaussian PDF without a shadowing effect $\chi_1(u, v)$ is also Gaussian (9).

2.2. Scalar approximation

The scalar approximation consists of approximating the Kirchhoff integral by a series expansion about the origin of the slopes and retains only the first-order term. Using (1) and (12.49) of [1], the scattering coefficient σ_{pq}^{SA} can be written as [1]

$$\sigma_{pq}^{SA} = \frac{|k|^2}{4\pi A_0}\langle|I_{SA}|^2\rangle \quad (10)$$

with

$$\langle|I_{SA}|^2\rangle = \iiiint \exp\{\mathrm{j}[q_x(x' - x'') + q_y(y' - y'')]\}\langle\cdots\rangle_{SA}\,\mathrm{d}x'\,\mathrm{d}y'\,\mathrm{d}x''\,\mathrm{d}y'' \quad (10a)$$

and

$$\langle\cdots\rangle_{SA} = \langle(|a_0|^2 + a_0^*a_1\gamma_x + a_0a_1^*\gamma_x' + a_0^*a_2\gamma_y + a_0a_2^*\gamma_y')\exp[\mathrm{j}q_z(z' - z'')]\rangle \quad (11)$$

where the symbol $*$ denotes the complex conjugate. $\{\gamma_x, \gamma_x'\}$, $\{\gamma_y, \gamma_y'\}$ are the surface slopes at points $\{x, x'\}$ and $\{y, y'\}$, respectively. Comparing the stationary phase method (6) with (10), the ensemble average $\langle\cdots\rangle_{SA}$ depends on the surface heights $\{z', z''\}$ as the stationary phase, and on the surface slopes $\{\gamma_x, \gamma_x', \gamma_y, \gamma_y'\}$. Note that the factor q^2/q_z^2 in (7) has been set equal to one, since the square of surface slopes has been neglected in comparison with unity. The terms $\{a_0, a_1, a_2\}$ depend on the problem geometry and are given in [1, p 941].

Using the same method as the stationary phase, we can write

$$\langle|I_{SA}|^2\rangle = \int_{-2L}^{2L}\int_{-2L}^{2L}(2L - |u|)(2L - |v|)\exp(\mathrm{j}q_xu + \mathrm{j}q_yv)\langle\cdots\rangle_{SA}\,\mathrm{d}u\,\mathrm{d}v. \quad (12)$$

It is important to note that Ulaby *et al* do not make the integrations over the slopes of $\langle\cdots\rangle_{SA}$, which are obtained from the $\chi_1(u, v)$ term. Therefore, the effects of the cross-correlation over the slopes and the heights are not treated.

3. Derivations of the surface height joint characteristic function and expected values

In the monostatic case (transmitter and receiver at the same location), the shadowing function characterizes the surface fraction which is visible from the receiver. In the bistatic case (transmitter and receiver at different locations), the surface fraction is visible from both the transmitter and the receiver. A study regarding the shadowing function has been done by Smith [13, 14] and Wagner [16]. These authors determined the shadowing function for a one-dimensional stationary stochastic process. Bourlier *et al* [15, 23] extended their results for a two-dimensional stationary surface by including the correlation between the surface heights and slopes. Bourlier also noted that Smith's results are more accurate than Wagner's.

Sancer [17] studied the shadowing effect on the Kirchhoff approach, and he showed that under the geometrical optics approximation, the statistical shadowing function is independent of the scattering coefficient. Strictly speaking, according to (8) this assumption is verified if the statistical shadowing function does not depend on the surface elevations. Since it is not the case, in this section, the effect of Smith's uncorrelated shadowing function on the surface height joint characteristic function (8), and the ensemble average (11), are investigated, for any configuration (monostatic, bistatic, isotropic and two-dimensional surfaces).

3.1. Smith statistical shadowing function

For a one-dimensional uncorrelated Gaussian process, the monostatic statistical shadowing function is (equation (22) of [13])

$$S_S(z',\gamma)=\left[1-\frac{1}{2}\operatorname{erfc}\left(\frac{z'}{\omega\sqrt{2}}\right)\right]^{\Lambda(v)}\Upsilon(\mu-\gamma) \tag{13}$$

with

$$\Lambda(v)=\frac{\mathrm{e}^{-v^2}-v\sqrt{\pi}\operatorname{erfc}(v)}{2v\sqrt{\pi}} \qquad v=\frac{\mu}{\sqrt{2}\sigma}=\frac{\cot|\theta|}{\sqrt{2}\sigma} \tag{13a}$$

and

$$\Upsilon(\mu-\gamma)=\begin{cases}0 & \text{if} \quad \gamma\geqslant\mu\\ 1 & \text{if} \quad \gamma<\mu\end{cases} \qquad \mu=\cot|\theta| \tag{13b}$$

with μ the incident beam slope, θ the incidence angle, σ the surface RMS slope, and erfc the complementary error-function. The term $\Upsilon(\mu-\gamma)$ carries a restriction over the slope.

For a one-dimensional bistatic case, equation (13) becomes [15]

$$S_S(z',\gamma)=\begin{cases}\left[1-\frac{1}{2}\operatorname{erfc}\left(\frac{z'}{\omega\sqrt{2}}\right)\right]^{\Lambda+\Lambda_s}\Upsilon(\mu+\gamma)\Upsilon(\mu_s-\gamma) & \text{for} \quad 0\leqslant v_s<\infty\\ \left[1-\frac{1}{2}\operatorname{erfc}\left(\frac{z'}{\omega\sqrt{2}}\right)\right]^{\Lambda_s}\Upsilon(\mu_s+\gamma) & \text{for} \quad -v\leqslant -v_s<0\\ \left[1-\frac{1}{2}\operatorname{erfc}\left(\frac{z'}{\omega\sqrt{2}}\right)\right]^{\Lambda}\Upsilon(\mu+\gamma) & \text{for} \quad -\infty\leqslant -v_s<-v\end{cases} \tag{14}$$

with

$$\mu_s=\cot|\theta_s| \qquad v_s=\frac{\cot|\theta_s|}{\sqrt{2}\sigma} \qquad \Lambda_s=\Lambda(v_s). \tag{14a}$$

Since the transmitter is defined according to $y < 0$, in the term $\Upsilon(\mu + \gamma)\Upsilon(\mu_s - \gamma)$, the sign of γ is positive with μ. Equation (14) involves $\theta \in [-\pi/2; 0]$ and $\theta_s \in [-\pi/2; \pi/2]$.

The monostatic and bistatic two-dimensional configurations [15] are obtained from the one-dimensional ones by replacing $\{v, v_s\}$ in (13*a*) and (14*a*) by

$$v = \frac{\cot|\theta|}{\sqrt{2[\alpha + \beta\cos(2\varphi)]}} \qquad v_s = \frac{\cot|\theta_s|}{\sqrt{2[\alpha + \beta\cos(2\varphi_s)]}} \tag{15}$$

with

$$\alpha = \frac{\sigma_x^2 + \sigma_y^2}{2} \qquad \beta = \frac{\sigma_x^2 - \sigma_y^2}{2} \tag{16}$$

and in the Υ function, γ is replaced by the surface slope γ_X defined either with respect to the azimuthal direction of the transmitter or the receiver. $\{\sigma_x^2, \sigma_y^2\}$ denote the surface slope variances in up x and y cross directions (see figure 1). The azimuthal angles $\{\varphi, \varphi_s\}$ represent the transmitter and receiver azimuthal directions according to the direction $(0x)$.

Finally, in the general case the statistical shadowing function can be written as

$$S_S(z', \gamma) = \left[1 - \frac{1}{2}\operatorname{erfc}\left(\frac{z'}{\omega\sqrt{2}}\right)\right]^{\Lambda'} \Upsilon' \tag{17}$$

where Λ' and Υ' are determined by identifying (17) with (13) and (14).

3.2. The stationary phase case

Since the surface height joint characteristic function is independent of the surface slope γ, the term Υ' of (17) will be studied later. In [12], for a monostatic configuration, the determination of the surface height joint probability density with shadowing effect $p_s(z', z'')$ has been investigated. Since with a bistatic configuration the Smith shadowing function keeps a similar form to that obtained for a monostatic configuration, the surface height joint characteristic function with shadow χ_{S1} is expressed as follows (equation (C8) of [12])

$$\chi_{S1}(\delta) = F(\delta)F^*(\delta) = |F(\delta)|^2 \tag{18}$$

with

$$F(\delta) = \frac{1}{\sqrt{\pi}}\int_{-\infty}^{\infty} \exp(\mathrm{j}\delta Z)\exp(-Z^2)\left[1 - \tfrac{1}{2}\operatorname{erfc}(Z)\right]^{\Lambda'} \mathrm{d}Z \tag{18a}$$

and

$$\delta(u, v) = q_z\omega\sqrt{2}[1 - f_0(u, v)]^{1/2}. \tag{18b}$$

If the shadowing effect is ignored corresponding to $\Lambda' = 0$, equation (18) becomes (9). If $\delta = 0$ then

$$\chi_{S10}(u, v) = 1/(\Lambda' + 1)^2. \tag{19}$$

This corresponds to the case where the shadowing effect is assumed to be statistically independent of the surface height PDF.

According to $\Lambda' = \{0, 1, 5\}$, figure 2 depicts the integrand absolute value $\exp(-Z^2)[1 - \operatorname{erfc}(Z)/2]^{\Lambda'}$ of (18*a*) versus Z, denoting the normalized surface height by $\omega\sqrt{2}$. Since Λ' increases, the distribution maximum is shifted toward the positive heights and the peak width decreases. For $\Lambda' = 0$ corresponding to the case where the shadow is ignored, the distribution is symmetric. For example, in the one-dimensional monostatic configuration with

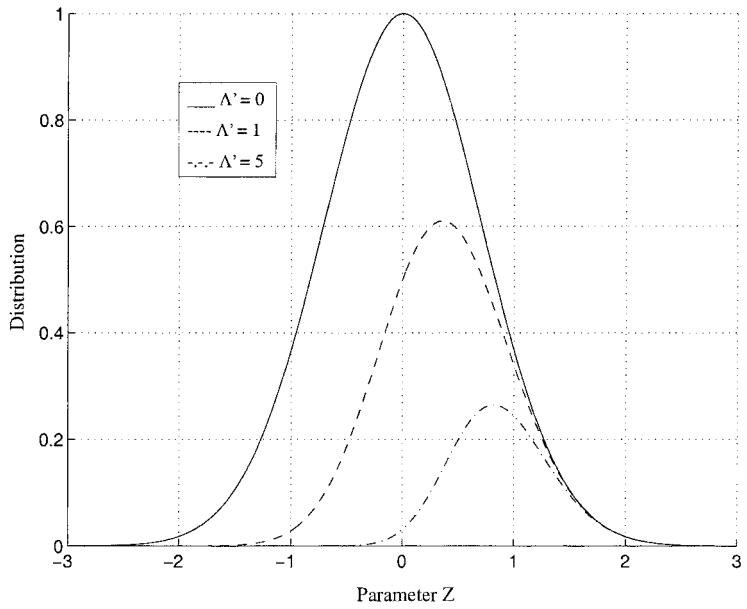

Figure 2. Distribution of the integrand versus the Z-normalized surface height.

$\Lambda' = \Lambda = \{0, 1, 5\}$, equation (13*a*) leads to $v = \{\infty, 0.1952, 0.0514\}$. Thus, with a surface RMS slope $\sigma = 0.4$, figure 2 represents the surface height distribution for incidence angles $\theta = a\cot(v\sqrt{2}\sigma) = \{0, 83.7, 88.3\}^\circ$. Consequently, the shadowing effect increases with the incidence angle, since it is equal to the percentage of the illuminated surface.

In the literature, the shadowing function is assumed to be statistically independent of the scattering coefficient leading to ((9) multiplied by (19))

$$\chi_{L1} = \exp(-\delta^2/2)/(\Lambda' + 1)^2. \tag{20}$$

Figure 3 plots the surface height joint characteristic functions χ_{S1} (full curve) and χ_{L1} (broken curve) versus the parameter δ for $\Lambda' = \{0, 5, 10, 15, 20\}$. For $\delta = 0$ we have $\chi_{S1} = \chi_{L1} = \chi_{S10} = 1/(\Lambda' + 1)^2$ (19), which means that the characteristic function decreases with Λ'. It is seen that $\{\chi_{S1}, \chi_{L1}\}$ are inversely proportional to δ and $\chi_{L1} \leqslant \chi_{S1}$, meaning that if the shadowing effect is taken into account through (20) then the results are underestimated. Unfortunately, equation (18*a*) cannot be integrated analytically.

Since the partial derivatives of the surface slopes have been replaced by the components of the phase (5), the scattering coefficient is independent of the surface slopes. Therefore, its average over the surface slopes is not required, and the statistical shadowing function with respect to the slopes can be introduced independently of the scattering coefficient calculation. Consequently, the expected value of (14) gives for a Gaussian process with zero mean, slope variance σ^2 [15]

$$\Pi(v, v_s) = \begin{cases} 1 - \frac{1}{2}[\operatorname{erfc}(v) + \operatorname{erfc}(v_s)] & \text{for} \quad 0 \leqslant v_s < \infty \\ 1 - \frac{1}{2}\operatorname{erfc}(v_s) & \text{for} \quad -v \leqslant -v_s < 0 \\ 1 - \frac{1}{2}\operatorname{erfc}(v) & \text{for} \quad -\infty \leqslant -v_s < -v \end{cases} \tag{21}$$

where $\{v, v_s\}$ are given by (13*a*) and (14*a*). For a two-dimensional surface, $\{v, v_s\}$ are replaced by (15).

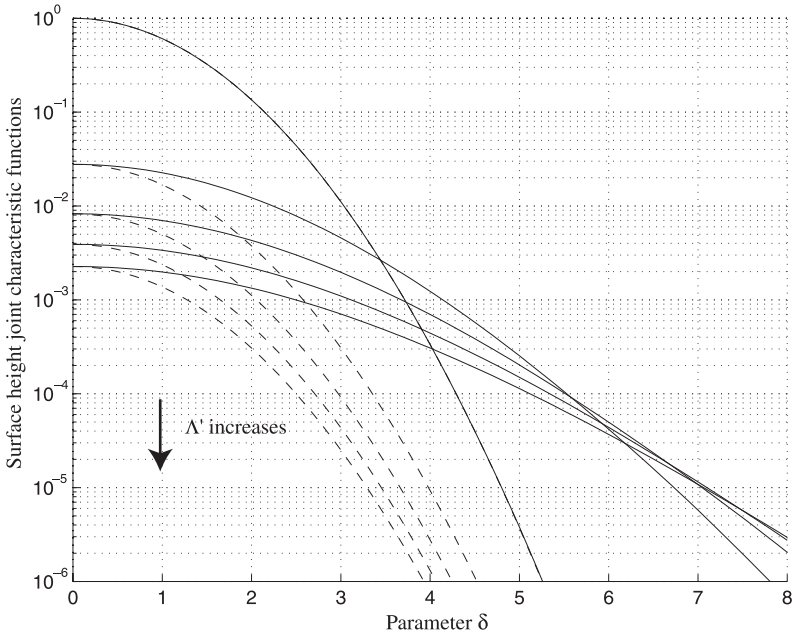

Figure 3. The surface height joint characteristic functions χ_{S1} (equation (18), full curve) and χ_{L1} (equation (20), broken curve) versus $\delta = q_z\omega\sqrt{2}(1-f_0)^{1/2}$ according to $\Lambda' = \{0, 5, 10, 15, 20\}$.

3.3. The scalar approximation case

In contrast to the stationary phase, the ensemble average (11) requires integrations over the slopes and it is given by

$$\langle\cdots\rangle_{SA}\iiiiint\left(|a_0|^2 + a_0^*a_1\gamma_x + a_0a_1^*\gamma_x' + a_0^*a_2\gamma_y + a_0a_2^*\gamma_y'\right) \times \exp[\mathrm{j}q_z(z'-z'')]p(\vec{V}_{xy})\,\mathrm{d}\vec{V}_{xy} \tag{22}$$

where the probability density $p(\vec{V}_{xy})$ of vector $\vec{V}_{xy}^T = [z'z''\gamma_x\gamma_x'\gamma_y\gamma_y']$ is the surface height and slope joint probability density defined in Cartesian coordinates $\{u = r\cos(\Phi),\ v = r\sin(\Phi)\}$. Since the $p(\vec{V}_{XY})$ probability density expressed from equation (11) of [12] is known in polar coordinates, the integral has to be determined in polar coordinates. Thus, making a rotation of Φ, we obtain

$$\begin{aligned} \gamma_x &= \gamma_X\cos\Phi - \gamma_Y\sin\Phi \qquad & \gamma_x' &= \gamma_X'\cos\Phi - \gamma_Y'\sin\Phi \\ \gamma_y &= \gamma_X\sin\Phi + \gamma_Y\cos\Phi \qquad & \gamma_y' &= \gamma_X'\sin\Phi + \gamma_Y'\cos\Phi \end{aligned} \tag{23}$$

and the integral (22) with the Jacobian equal to one becomes

$$\langle\cdots\rangle_{SA} = \iiiiint\left(|a_0|^2 + A_1\gamma_X + A_1^*\gamma_X' + A_2\gamma_Y + A_2^*\gamma_Y'\right) \times \exp[\mathrm{j}q_z(z'-z'')]p(\vec{V}_{XY})\,\mathrm{d}\vec{V}_{XY} \tag{24}$$

with

$$\begin{aligned} A_1 &= a_0(a_1\cos\Phi + a_2\sin\Phi) = a_0a\cos(\varphi-\Phi) \\ A_2 &= a_0(a_2\cos\Phi - a_1\sin\Phi) = a_0a\sin(\varphi-\Phi) \end{aligned} \tag{24a}$$

where the coefficient a is given in [1, p 941]. The derivation of (24) requires knowledge of the following expected values $\{E_4(\gamma_X), E_4(\gamma_X'), E_4(\gamma_Y), E_4(\gamma_Y')\}$ defined as

$$E_4(\cdots) = \int\int\int\int (\cdots) p(\vec{V}_{XY})\, \mathrm{d}\gamma_X\, \mathrm{d}\gamma_X'\, \mathrm{d}\gamma_Y\, \mathrm{d}\gamma_Y'. \tag{25}$$

When the shadow is ignored, equations (A11)–(A13) of [12] lead to

$$\begin{aligned} E_4(\gamma_X') &= -\frac{\sigma_X f_1(z' - z'' f_0)}{\omega(1 - f_0^2)} p(z', z'') \qquad & E_4(\gamma_X) &= \frac{\sigma_X f_1(z'' - z' f_0)}{\omega(1 - f_0^2)} p(z', z'') \\ E_4(\gamma_Y') &= -\frac{\sigma_Y f_{16}(z' - z'' f_0)}{\omega(1 - f_0^2)} p(z', z'') \qquad & E_4(\gamma_Y) &= \frac{\sigma_Y f_{16}(z'' - z' f_0)}{\omega(1 - f_0^2)} p(z', z'') \end{aligned} \tag{26}$$

where $\{f_0, f_1, f_{16}, \omega, \sigma_X, \sigma_Y\}$ are elements of the covariance matrix expressed from equation (12) of [12]

$$\begin{aligned} &R_0 = R_{00} - \cos(2\Phi) R_{02} \\ &R_1 = R_{10} - \cos(2\Phi) R_{12} \qquad \text{with} \quad R_{ij} = \frac{\mathrm{d}^i R_{0j}}{\mathrm{d}r^i} \\ &C_{16} = \frac{2R_{02}\sin(2\Phi)}{r} \\ &\sigma_X^2 = \alpha + \beta\cos(2\Phi) \qquad \sigma_Y^2 = \alpha - \beta\cos(2\Phi) \\ &f_0 = R_0/\omega^2 \qquad f_1 = -R_1/(\omega\sigma_X) \qquad f_{16} = -C_{16}/(\omega\sigma_Y) \end{aligned} \tag{26a}$$

with f_0 the surface normalized height two-dimensional autocorrelation function of height variance $\omega^2 = R_{00}(0)$, $\{\sigma_X^2, \sigma_Y^2\}$ the surface slope variances in $\{(0X), (0Y)\}$ directions, and $\{\alpha, \beta\}$ given by (16). R_0 corresponds to the general representation of ocean-like autocorrelation [19, 20], where Φ denotes the wind direction.

In section 4, R_0 will be introduced in the determination of the scattering coefficient. $\{R_1, C_{16}\}$ quantified the correlation between the heights and the slopes in the $\{(0X), (0Y)\}$ directions, respectively. $p(z', z'')$ is the surface height joint probability expressed as

$$p(z', z'') = \frac{1}{2\pi\omega^2(1 - f_0^2)^{1/2}} \exp\left[-\frac{1}{2\omega^2(1 - f_0^2)}(z'^2 + z''^2 - 2f_0 z' z'')\right]. \tag{27}$$

Substituting (27), (26) into (24), and performing the integrations over the surface elevations $\{z', z''\}$, we show that the ensemble without a shadow is

$$\langle\cdots\rangle_{SA} = \chi_1\left\{|a_0|^2 - 2\mathrm{j}q_z\omega\,\mathrm{Re}(a_0 a)[\sigma_X f_1\cos(\varphi - \Phi) + \sigma_Y f_{16}\sin(\varphi - \Phi)]\right\} \tag{28}$$

where χ_1 is given by (9) and Re denotes the real part.

As shown by Bourlier *et al* [12], the derivation of the expected values E_{S4} with a shadow requires the eigenvalues and eigenvectors analytical determination of the covariance matrix $[C_{XY}]$ of dimension six. Moreover, they require the integrations over the slopes $\{\gamma_X, \gamma_X', \gamma_Y, \gamma_Y'\}$ over $\{]-\infty; \mu],]-\infty; \mu],]-\infty; \infty[,]-\infty; \infty[\}$ ranges and the integration over the heights multiplied by the exponential term $\exp[\mathrm{j}q_z(z' - z'')]$. To solve the problem analytically, the cross-correlation between the heights and the slopes quantified by $\{R_1, C_{16}\}$ is assumed to be negligible. We show then in appendix A, that the ensemble average with shadow $\langle\cdots\rangle_{SA}^S$ in polar coordinates is expressed as follows:

$$\langle\cdots\rangle_{SA}^S = [B_0 - \mathrm{j}B_c\cos(\varphi - \Phi) - \mathrm{j}B_s\sin(\varphi - \Phi)]\chi_{S1} \tag{29}$$

where $\{B_0, B_c, B_s\}$ are given by (A25).

4. Incoherent scattering coefficient with and without shadow

In this section, the investigation is effected with and without incoherent scattering coefficient by using the stationary phase and scalar approximation. Next, the models are compared with experimental data [18].

4.1. Incoherent scattering coefficient

Substituting (7) into (6) and assuming either that the illuminated surface size is infinite or much larger than the correlation length, the variable transformations $\{u = r\cos\Phi,\ v = r\sin\Phi\}$ lead to the following scattering coefficient with the stationary phase (exponent SP):

$$\sigma_{pq}^{SP} = \frac{\Pi|q^2 U'_{pq}|^2}{4\pi q_z^2}\int_0^\infty r\,\mathrm{d}r\left\{\int_0^{2\pi}\exp\left[\mathrm{j}r\sqrt{q_x^2+q_y^2}\cos(\Phi-\varphi)\right]\right.$$
$$\left.\times\chi_{1,S1}(q_z\omega\sqrt{2}[1-f_0(r,\Phi)]^{1/2})\,\mathrm{d}\Phi\right\} \tag{30}$$

with

$$\phi = \arctan(q_y/q_x) \qquad |U'_{pq}|^2 = \left|\frac{kU_{pq}}{q}\right|^2 \tag{30a}$$

where Π is given by (21). If the shadow is ignored then χ_1 (9) is taken with $\Pi = 1$ else χ_{1S} (18) is considered.

The scattered intensities from a random surface can in general be decomposed into coherent and incoherent components. Coherent component σ_{pqC} (index C) mostly contributes in the specular reflected component, whereas the incoherent component σ_{pqI} (index I) contributes in all directions, and we can write [24]

$$\sigma_{pqI} = \sigma_{pq} - \sigma_{pqC} \tag{31}$$

where the coherent component σ_{pqC} is calculated from averaging $|\langle I_{SP}\rangle|^2$ (2*a*) and we obtain

$$\sigma_{pqC}^{SP} = \frac{\Pi|q^2 U'_{pq}|^2}{4\pi q_z^2}\int_0^\infty r\,\mathrm{d}r\left\{\int_0^{2\pi}\exp\left[\mathrm{j}r\sqrt{q_x^2+q_y^2}\cos(\Phi-\varphi)\right]\chi_{1,S1}(q_z\omega\sqrt{2})\,\mathrm{d}\Phi\right\}. \tag{32}$$

Since the ensemble average $\langle I_{SP}\rangle$ is only over z', $\chi(q_z\omega\sqrt{2})$ is independent of the surface height normalized autocorrelation function $f_0(r,\Phi)$. Consequently, the incoherent scattering is expressed as

$$\sigma_{pqI}^{SP} = \frac{\Pi|q^2 U'_{pq}|^2}{4\pi q_z^2}\int_0^\infty r\,\mathrm{d}r\left\{\int_0^{2\pi}\exp\left[\mathrm{j}r\sqrt{q_x^2+q_y^2}\cos(\Phi-\varphi)\right]\right.$$
$$\left.\times[\chi_{1,S1}(q_z\omega\sqrt{2}[1-f_0(r,\Phi)]^{1/2}) - \chi_{1,S1}(q_z\omega\sqrt{2})]\,\mathrm{d}\Phi\right\}. \tag{33}$$

Comparing (7) with (12), and using (33), the incoherent scattering coefficient under the scalar approximation (exponent SA) is expressed as

$$\sigma_{pqI}^{SA} = \frac{|k|^2}{4\pi}\int_0^\infty r\,\mathrm{d}r\left\{\int_0^{2\pi}\exp\left[\mathrm{j}r\sqrt{q_x^2+q_y^2}\cos(\Phi-\varphi)\right]\right.$$
$$\left.\times\left[\chi_{1,S1}(q_z\omega\sqrt{2}[1-f_0(r,\Phi)]^{1/2})\chi'_{1,S1} - \chi_{1,S1}(q_z\omega\sqrt{2})\chi'_{10,S10}\right]\mathrm{d}\Phi\right\} \tag{34}$$

where χ_1' is obtained from (28) in the case where the shadow is ignored

$$\chi_1' = |a_0|^2 - 2\mathrm{j}q_z\omega\,\mathrm{Re}(a_0 a)[\sigma_X f_1\cos(\varphi-\Phi)+\sigma_Y f_{16}\sin(\varphi-\Phi)] \tag{34a}$$

and χ_{S1}' is obtained from (29) in the case where the shadow is included

$$\chi_{S1}' = B_0 - \mathrm{j}B_c\cos(\varphi-\Phi) - \mathrm{j}B_s\sin(\varphi-\Phi). \tag{34b}$$

χ_{10}' is determined by making in (34*a*) $\{f_1=0,\ f_{16}=0\}$, thus $\chi_{10}' = |a_0|^2$, whereas χ_{S10}' is computed by making in (34*b*) $\{f_2=0,\ f_{36}=0\}$ within (A25).

4.2. Incoherent scattering component from an isotropic rough surface

In this section, for an isotropic rough surface, we compare the incoherent scattering coefficient with and without shadow. For an isotropic surface, the surface-height-normalized autocorrelation function $f_0(r,\Phi)$ is independent of the azimuthal direction Φ, which gives from (26*a*) that $R_{02}=0, \sigma_X=\sigma_Y, \sigma_{XY}=0$, meaning that $f_{16}=0$ and from (A17) $f_{36}=0$.

With the variable transformation $u = r/L_c$ (L_c denotes the surface correlation length), the integration over Φ leads from (33) to

$$\sigma_{SI}^{SP} = \frac{\Pi|q^2U_{pq}'|^2L_c^2}{2q_z^2}\int_0^\infty uJ_0\Big(uL_c\sqrt{q_x^2+q_y^2}\Big) \times\Big\{\chi_{S1}(q_z\omega\sqrt{2}[1-f_0(u)]^{1/2}) - \chi_{S1}(q_z\omega\sqrt{2})\Big\}\,\mathrm{d}u \tag{35}$$

with J_0 the zeroth-order Bessel function, and χ_{S1} given by (18). The index notation pq is substituted by S (shadow).

If the shadow is ignored (index US), then $\Pi=1$ and χ_1 is equal to (9) which leads to

$$\sigma_{USI}^{SP} = \frac{|q^2U_{pq}'|^2L_c^2}{2q_z^2}\exp(-q_z^2\omega^2)\int_0^\infty uJ_0\Big(uL_c\sqrt{q_x^2+q_y^2}\Big)\Big\{\exp[q_z^2\omega^2 f_0(u)]-1\Big\}\,\mathrm{d}u. \tag{36}$$

Using a series representation for the factor $\exp(q_z^2\omega^2 f_0)$ with Gaussian ($\exp(-r^2/L_c^2)$) surface height autocorrelation function, we obtain by performing the integration over u,

$$\sigma_{USI}^{SP} = \frac{\Pi|q^2U_{pq}'|^2L_c^2}{4q_z^2}\exp(-q_z^2\omega^2)\sum_{n=1}^{\infty}\frac{(q_z\omega)^{2n}}{nn!}\exp\left[-\frac{L_c^2(q_x^2+q_y^2)}{4n}\right]. \tag{37}$$

If the statistical shadowing function is assumed to be independent (index IN) of the surface height PDF, which is similar to considering that the characteristic function is equal to (20), then the incoherent (index I) scattering coefficient is expressed as

$$\sigma_{INI}^{SP} = \sigma_{USI}^{SP}\frac{\Pi}{(\Lambda'+1)^2}. \tag{38}$$

If $q_z\omega$ is much greater than one, then the incoherent scattering with shadowing effect is obtained from the geometrical optics (exponent OG) solution [1]

$$\sigma_I^{OG} = \frac{\Pi}{(\Lambda'+1)^2}\frac{q^4|U_{pq}'|^2}{2q_z^4\sigma_X^2}\exp\left(-\frac{q_x^2+q_y^2}{2q_z^2\sigma_X^2}\right). \tag{39}$$

Since for an isotropic surface we have $f_{16}=0$, the incoherent scattering coefficient with the scalar approximation becomes, when the shadow is ignored,

$$\sigma_{USI}^{SA} = \frac{|k|^2}{4\pi}\exp(-q_z^2\omega^2)\int_0^\infty r\,\mathrm{d}r\Bigg\{\int_0^{2\pi}\exp\Big[\mathrm{j}r\sqrt{q_x^2+q_y^2}\cos(\Phi-\varphi)\Big] \times\Big(\exp[q_z^2\omega^2 f_0(u)][|a_0|^2 - 2\mathrm{j}q_z\omega\,\mathrm{Re}(a_0a)\sigma_X f_1\cos(\varphi-\Phi)] - |a_0|^2\Big)\,\mathrm{d}\Phi\Bigg\}. \tag{40}$$

Table 1. Expression of elements of the one-dimensional scattering coefficient for a Gaussian surface height autocorrelation function with slope variance $\sigma_X^2 = 2\omega^2/L_c^2$ when the transmitter and receiver are located in the same plane ($\varphi_s = \varphi$).

Elements	Bistatic configuration
$\{\vec{h}_s \cdot \vec{n}_i, \vec{h}_i \cdot \vec{n}_s, \vec{v}_s \cdot \vec{n}_i, \vec{v}_i \cdot \vec{n}_s\}$	$\{0, 0, \sin(\theta - \theta_s), \sin(\theta - \theta_s)\}$
$\{r_1, r_2, r_3, r_4\}$	$\{0, \sin^2(\theta - \theta_s), 0, 0\}$
θ_1	$\lvert(\theta - \theta_s)/2\rvert$
$\{\lvert U'_{h_s h_i}\rvert^2, \lvert U'_{v_s v_i}\rvert^2, \lvert U'_{h_s v_i}\rvert^2, \lvert U'_{v_s h_i}\rvert^2\}$	$\{\lvert R_H(\theta_1)^2\rvert, \lvert R_V(\theta_1)^2\rvert, 0, 0\}$
$q_z\omega$	$k\omega(\cos\theta + \cos\theta_s)$
$L_c^2(q_x^2 + q_y^2)$	$2(k\omega)^2(\sin\theta - \sin\theta_s)^2/\sigma^2$
$\lvert q\rvert^4 L_c^2/(2\lvert q_z\rvert^2)$	$\left\{\dfrac{2k\omega\cos[(\theta + \theta_s)/2]}{\sigma_X\cos[(\theta - \theta_s)/2]}\right\}^2$
$\{f_0, f_1, f_2\}$	$\{\exp(-u^2), u\sqrt{2}\exp(-u^2), \exp(-u^2)(1 - 2u^2)\}$
a_0 (scalar approximation)	$\{(\cos\theta + \cos\theta_s)R_H(\theta), (\cos\theta + \cos\theta_s)R_V(\theta), 0, 0\}$
a (scalar approximation)	$\{-(\cos\theta + \cos\theta_s)R_{H1}(\theta) - (\sin\theta - \sin\theta_s)R_H(\theta),$ $(\cos\theta + \cos\theta_s)R_{V1}(\theta) + (\sin\theta - \sin\theta_s)R_V(\theta), 0, 0\}$
$\cos(\phi - \varphi)$ (scalar approximation)	1
$\lvert k\rvert^2 L_c^2/2$ (scalar approximation)	$(k\omega/\sigma_X)^2$

From (B7) of appendix B, the integration over Φ with $u = r/L_c$ leads to

$$\sigma_{USI}^{SA} = \frac{|k|^2 L_c^2}{2}\exp(-q_z^2\omega^2)\int_0^\infty u\,\mathrm{d}u\left\{|a_0|^2 J_0\left(uL_c\sqrt{q_x^2 + q_y^2}\right)\{\exp[q_z^2\omega^2 f_0(u)] - 1\}\right.$$
$$\left. + 2J_1\left(uL_c\sqrt{q_x^2 + q_y^2}\right)q_z\omega\,\mathrm{Re}(a_0 a)\sigma_X f_1\right\}. \tag{41}$$

Since $\{\sigma_{XY} = 0,\ f_{36} = 0\}$, from (A25), we obtain $B_s = 0$. From (34), and applying the same method as previously, the incoherent scattering coefficient σ_{SI}^{SA} with shadow is

$$\sigma_{SI}^{SA} = \frac{|k|^2}{4\pi}\int_0^\infty r\,\mathrm{d}r\left\{\int_0^{2\pi}\exp\left[\mathrm{j}r\sqrt{q_x^2 + q_y^2}\cos(\Phi - \varphi)\right]\right.$$
$$\times\left[\chi_{S1}(q_z\omega\sqrt{2}[1 - f_0(r)]^{1/2})[B_0 - \mathrm{j}B_c\cos(\varphi - \Phi)]\right.$$
$$\left.\left. - \chi_{S1}(q_z\omega\sqrt{2})[B_{00} - \mathrm{j}B_{c0}\cos(\varphi - \Phi)]\right]\mathrm{d}\Phi\right\} \tag{42}$$

where $\{B_{00} = B_0,\ B_{c0} = B_c\}$ if $f_2 = 0$ in (A25). From (B7) of appendix B, the integration over Φ with $u = r/L_c$ leads to

$$\sigma_{SI}^{SA} = \frac{|k|^2 L_c^2}{2}\int_0^\infty u\,\mathrm{d}u\left\{J_0\left(uL_c\sqrt{q_x^2 + q_y^2}\right)\right.$$
$$\times\left\{\chi_{S1}(q_z\omega\sqrt{2}[1 - f_0(r)]^{1/2})B_0 - \chi_{S1}(q_z\omega\sqrt{2})B_{00}\right\}$$
$$\left. + J_1\left(uL_c\sqrt{q_x^2 + q_y^2}\right)\left\{\chi_{S1}(q_z\omega\sqrt{2}[1 - f_0(r)]^{1/2})B_c - \chi_{S1}(q_z\omega\sqrt{2})B_{c0}\right\}\right\}. \tag{43}$$

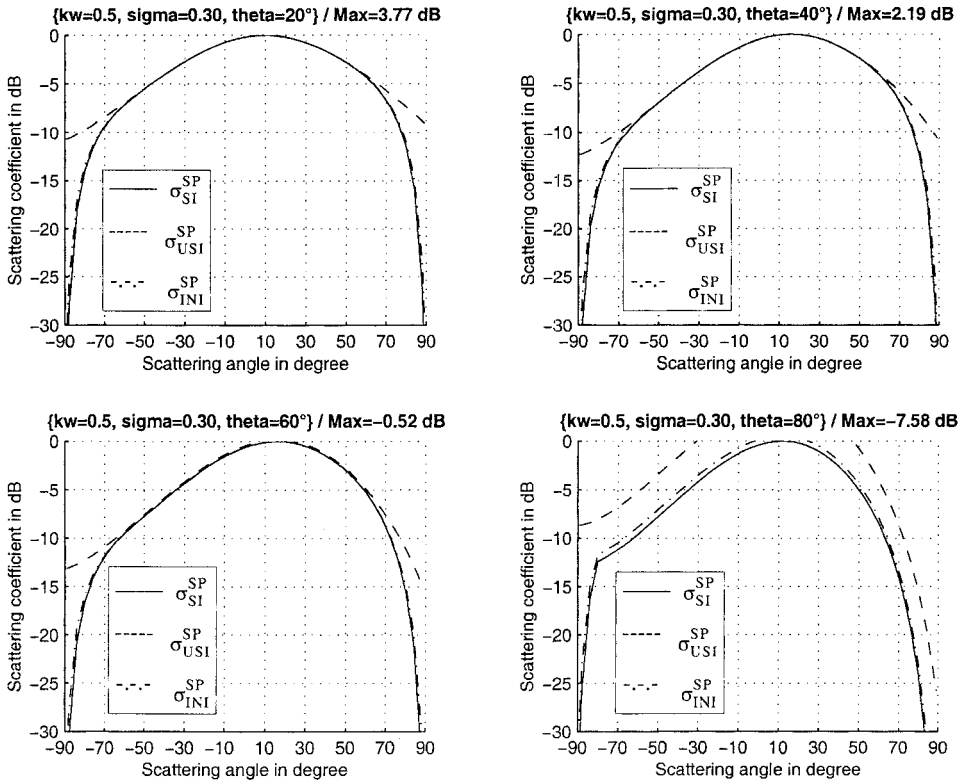

Figure 4. Normalized bistatic incoherent scattering coefficient in dB from a perfectly-conducting isotropic surface versus the scattering angle θ_s with respect to the incidence angle $|\theta| = \{20, 40, 60, 80\}^\circ$ with surface slope variance $\sigma_x = 0.3$ and $k\omega = 0.5$. The scattering coefficient is normalized by the maximum of σ_{SI}^{SP}. Full curve, σ_{SI}^{SP} (35) (stationary phase with shadow); broken curve, σ_{USI}^{SP} (36) (stationary phase without shadow) and chain curve, σ_{INI}^{SP} (38) (stationary phase with shadow assumed to be independent).

As for the stationary phase (38), we define the incoherent scattering coefficient when the statistical shadowing function is assumed to be independent of the surface height PDF, thus

$$\sigma_{INI}^{SA} = \sigma_{USI}^{SA} \frac{\Pi}{(\Lambda' + 1)^2}. \tag{44}$$

4.3. Simulations for an isotropic rough surface

An interesting case is when the transmitter and receiver are in the same plane ($\varphi_s = \varphi$). Monostatic and bistatic radar measurements fall into this category. From table 1, we can note that the depolarized scattering coefficients $\sigma^0_{h_s v_i, v_s h_i}$ are equal to zero because the multiple scattering is ignored. Moreover, we see that the scattering coefficient depends on $k\omega$ and σ_X.

Figures 4–6 represent the normalized incoherent bistatic scattering coefficient in dB ($10 \log_{10}(\cdots)$) from a perfectly-conducting isotropic surface versus the scattering angle θ_s according to the incidence angle $|\theta| = \{20, 40, 60, 80\}^\circ$ with surface RMS slope $\sigma_x = 0.3$ and $k\omega = \{0.5, 1, 4\}$. The incoherent scattering coefficient is normalized by the maximum of

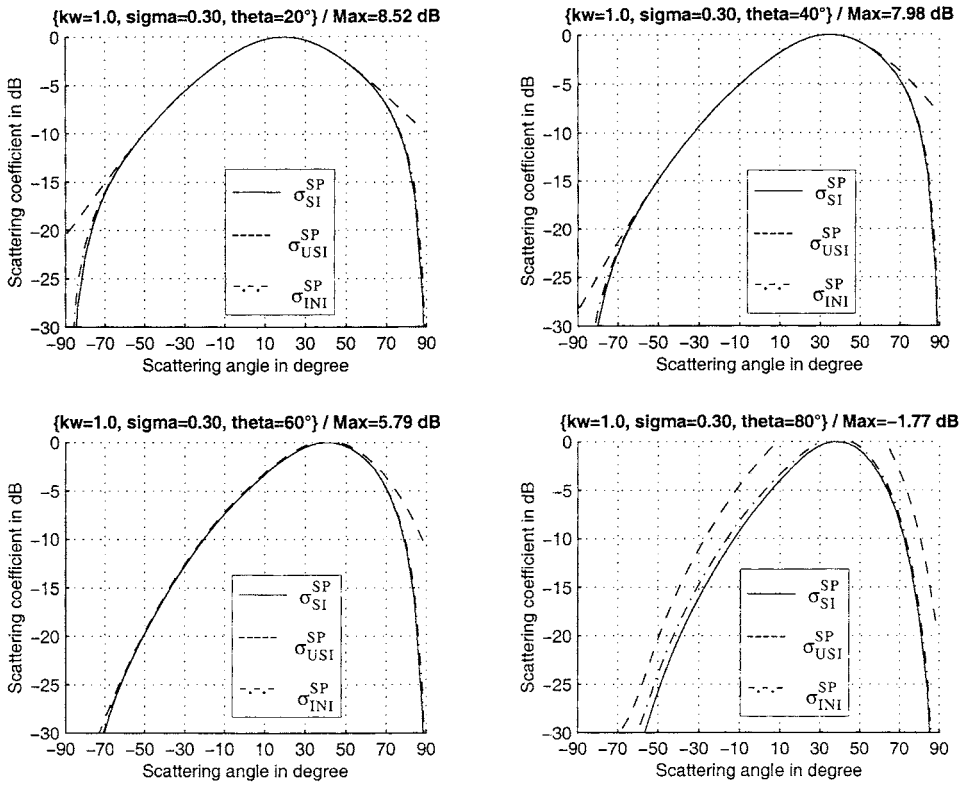

Figure 5. Same variation as figure 4 with $k\omega = 1$.

σ_{SI}^{SP}. The full curve is σ_{SI}^{SP} (35), broken curve is σ_{USI}^{SP} (36), chain curve is σ_{INI}^{SP} (38), and cross curve is σ_{I}^{GO} (39).

As depicted in figure 4, for a slightly rough surface $k\omega = 0.5$, the unshadowed scattering coefficient σ_{USI}^{SP} is in good agreement with σ_{SI}^{SP} and σ_{INI}^{SP} around the specular direction given by $\theta_s = |\theta|$. For grazing scattering angles the unshadowed scattering coefficient is overestimated since the shadowing effect is not negligible. From figures 5 and 6, this behaviour is significant with respect to the surface roughness $k\omega = \{1, 4\}$. Comparing figures 4 and 5 ($\sigma_x = 0.3$) with figures 7 and 8 ($\sigma_x = 0.1$), respectively, this overestimation decreases when the surface RMS slope σ_x decreases because the percentage of the hidden surface also decreases. As expected, the bistatic cross section drops off more slowly with increasing scattering angle as the surface RMS slope increases.

From figures 4–6 and comparing σ_{INI}^{SP} with σ_{SI}^{SP}, we can see that σ_{INI}^{SP} obtained from averaging the statistical shadowing function independently of the unshadowed bistatic cross section is slightly overestimated. This overestimation increases with the surface roughness $k\omega$ and the surface slope variance. Unlike the incoherent scattering coefficient, the total scattering coefficient characterized by figure 2, we have σ_{S}^{SP} greater than σ_{IN}^{SP}. As depicted in figure 6 with $k\omega = 4$, the geometrical optics solution with shadow σ_{I}^{GO} plotted in crosses is correct since this example falls in the high-frequency region. In general, since the shadowing effect is included, the bistatic cross section is not symmetrical according to the specular direction.

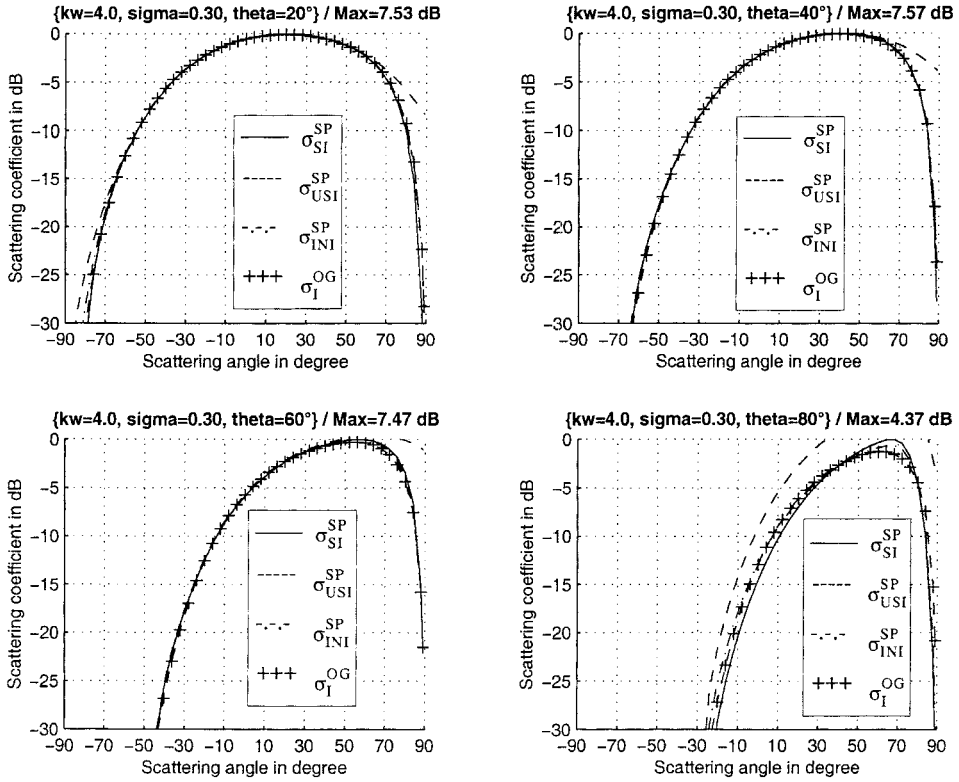

Figure 6. Same variation as figure 4 with $k\omega = 4$. Moreover, σ_I^{OG} (39) is plotted as crosses.

Table 2. Values of kL_c and kR_c of figures 4–8.

$k\omega$	0.5	1	4
kL_c with $\sigma = 0.1$	2.36	4.71	18.86
kR_c with $\sigma = 0.1$	3.77	7.54	30.17
kL_c with $\sigma = 0.3$	7.07	14.14	56.57
kR_c with $\sigma = 0.3$	35.97	71.92	287.70

The stationary phase approximation assumes that both $kL_c \gg 2\pi$ and $kR_c \gg 2\pi$, with R_c the surface mean curvature radius, which equal for a Gaussian surface height autocorrelation function with small slopes σ_X [21]

$$kR_c = \frac{kL_c}{1.95\sigma_X(1 + 3\sigma_X^2/4)}. \tag{45}$$

As shown in table 2, both criteria are approximately valid for the simulations of figures 4–8.

In figure 9, the bistatic incoherent scattering coefficient from the dielectric isotropic surface versus the scattering angle θ_s with respect to the surface permittivity $\varepsilon = \{$infinity (perfectly-conducting surface case), $60 - 40$j (sea case in band X), $1.5 - 0.5$j (optical case)$\}$ and the

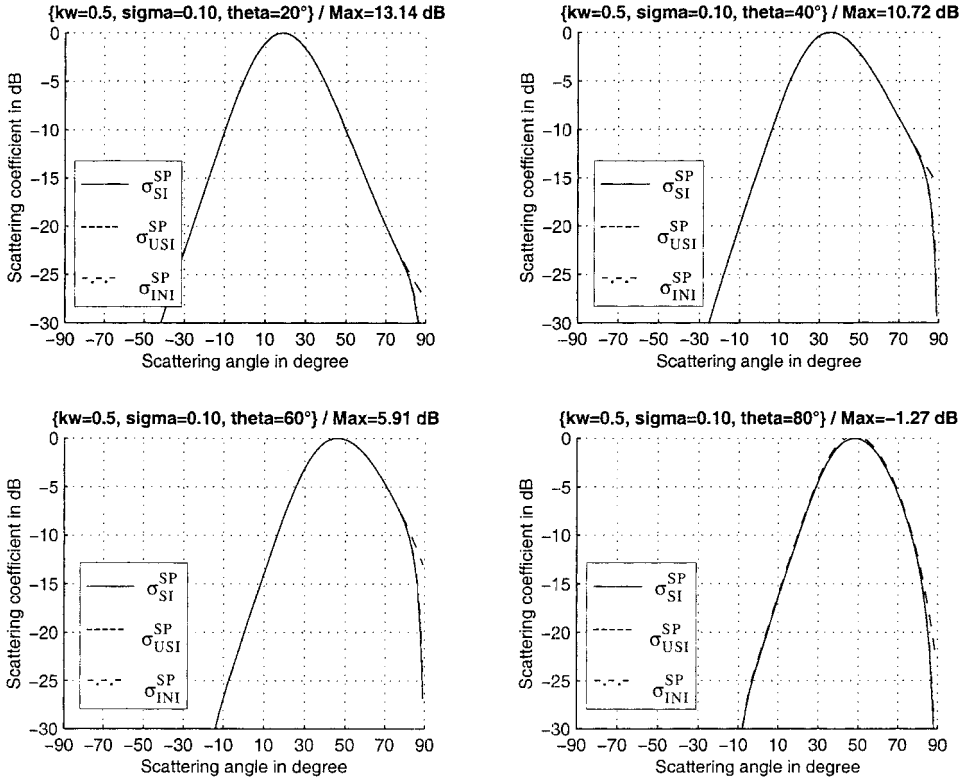

Figure 7. Same variation as figure 4 with $\sigma_x = 0.3$.

polarizations (VV or HH) with $|\theta| = 80^\circ$ is plotted. Full curve, σ_{SI}^{SP} (35) (stationary phase method with shadow) and crosses, σ_{SI}^{SA} (43) (scalar approximation with shadow). The surface parameters are similar to those in figure 8. We can see that when the permittivity increases, the incoherent component proportional to the squared modulus of the Fresnel coefficients decreases because the Fresnel coefficients are smaller. Their moduli are maxima for a perfectly-conducting surface corresponding to $\varepsilon_r \to \infty$. We can also note that there is no deviation between the two scattering models. In vertical polarization, the Brewster phenomenon is not observed, because Brewster's angle is close to 90° where the scattering coefficient is very small.

In figure 10, σ_{SI}^{SP}, σ_{INI}^{SP}, σ_{SI}^{SA} and σ_{INI}^{SA} (44) are compared with the experimental data σ_I^{EX} (see figures 5–8 in O'Donnell and Mendez [18] with $\sigma_x = 0.154$). In figure 10(a), $|\theta| = 20^\circ$, $k\omega = 22.532$, $kL_c = 207.424$, $kR_c = 679.81$. In figure 10(b), $|\theta| = 20^\circ$, $k\omega = 1.346$, $kL_c = 12.387$, $kR_c = 40.698$. Both of these cases are in the high-frequency limit range and kR_c is much larger than unity. The experimental data are not plotted because they are in good agreement with σ_{SI}^{SA} (figures 5 and 6 of [18]) slightly smaller than σ_{SI}^{SP}. We can see that $\sigma_{INI}^{SP} = \sigma_{SI}^{SP}$ and $\sigma_{INI}^{SA} = \sigma_{SI}^{SA}$, because the shadowing effect can be neglected.

The surface parameters of figure 10(c) are exactly the same as in figure 10(a). The only difference is in the incident angle. Although we have $\{kL_c, kR_c\}$ much greater than unity, for scattering angles smaller than the specular direction, the models deviate from the experimental data. Although the shadowing effect is included, at near-grazing scattering

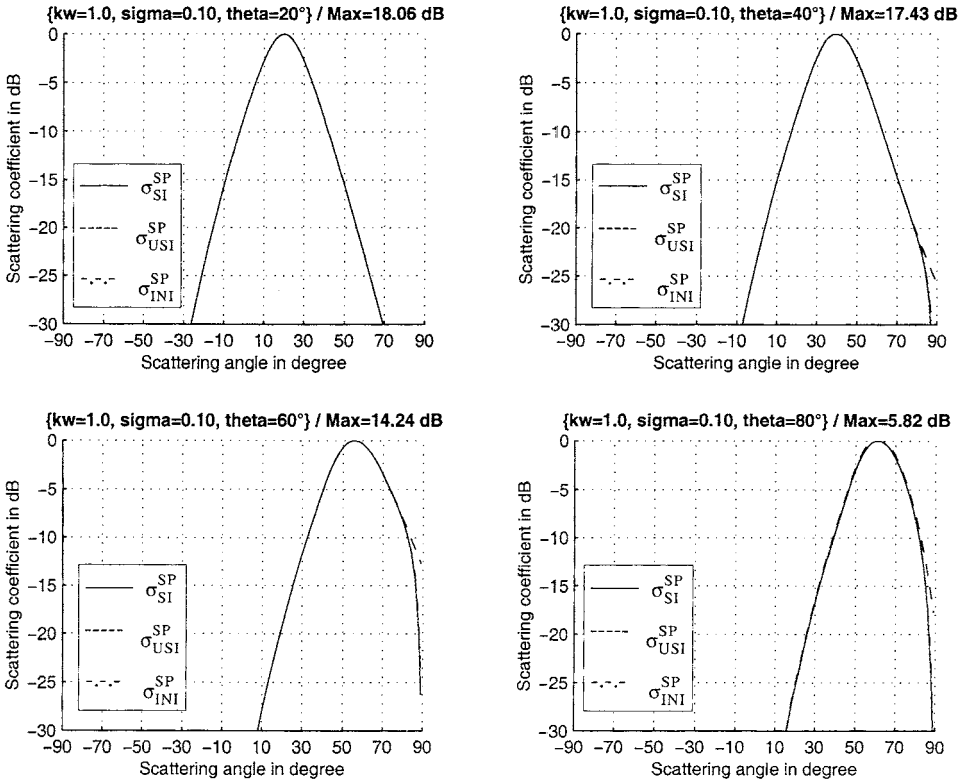

Figure 8. Same variation as figure 5 with $\sigma_x = 0.3$.

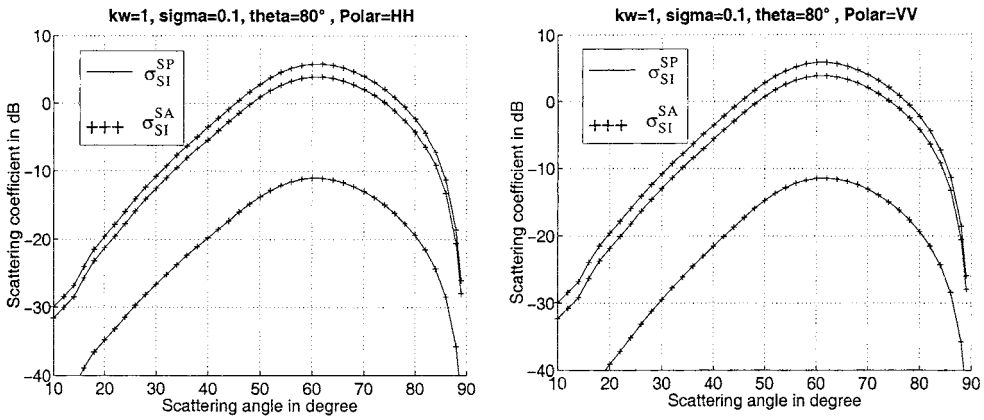

Figure 9. Bistatic incoherent scattering coefficient from a dielectric isotropic surface versus the scattering angle θ_s with respect to the surface permittivity $\varepsilon_r = \{\text{infinity}, 60 - 40\text{j}, 1.5 - 0.5\text{j}\}$ and the polarizations (VV or HH) with $|\theta| = 80^\circ$. Full curve is σ_{SI}^{SP} (35) (stationary phase method with shadow), and cross curve is σ_{SI}^{SA} (43) (scalar approximation with shadow). The surface parameters are similar to figure 8.

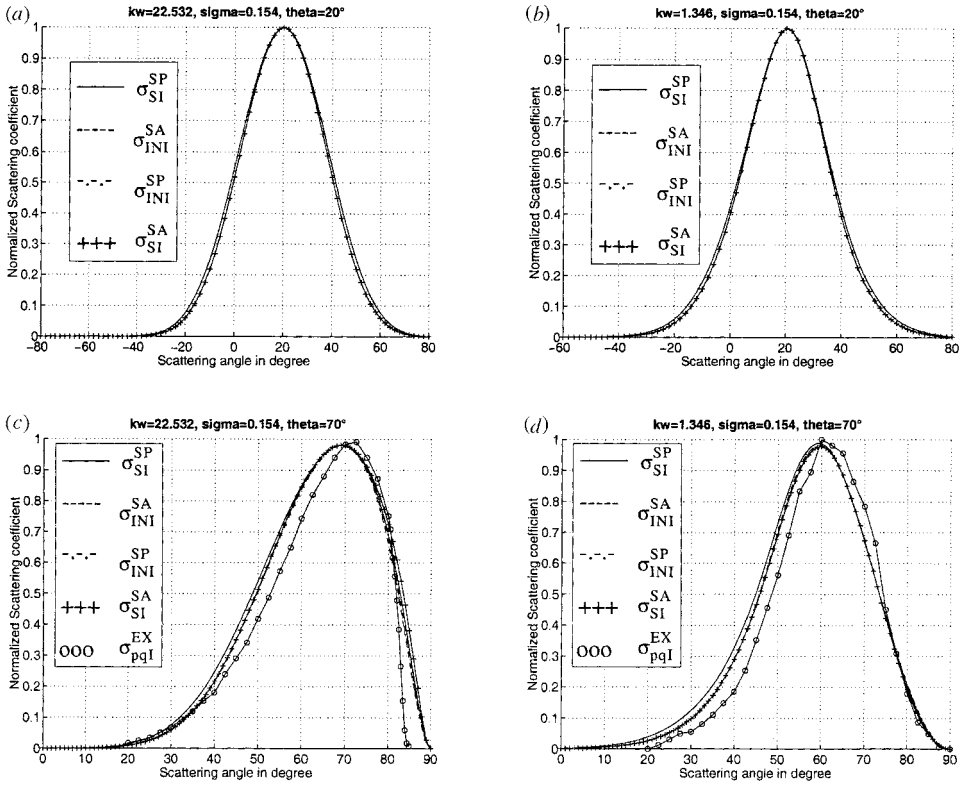

Figure 10. Comparison of models with the experimental data (see figures 5–8 in O'Donnell and Mendez [18]).

angles, an overestimation according to σ_I^{EX} is observed. Bahar and Lee [25] have also studied their full wave solution without shadow. From figure 16 of [25], it is observed that at near grazing angles, their model underestimates the bistatic cross section. They explain this deviation as being due to the fact that the experimental surface height autocorrelation function is not perfectly Gaussian. Indeed, it is observed as an oscillatory behaviour, which becomes significant at grazing angles.

The surface parameters of figure 10(d) are exactly the same as those found in figure 10(b) and $|\theta| = 70^\circ$. Similar to the case of figure 10(c), the results deviate from the experimental data, but they are correct for grazing angles.

When the shadowing function is introduced in the determination of the bistatic scattering coefficient obtained from the analytical Kirchhoff approximation, it is simply multiplied ([1, p 1024], [24, p 95], [7, equations (31)]) by either Smith's (index S) or Wagner's (index W) shadowing functions assumed to be independent of the surface height joint characteristic function. This assumption involves that the shadowed scattering coefficient is obtained from the product of the unshadowed scattering coefficient by a factor, which characterizes the shadowing effect expressed as follows:

$$S_S(v, v_s) = \Pi(v, v_s)\frac{1}{\Lambda' + 1} \qquad S_W(v, v_s) = \Pi(v, v_s)\frac{1 - \exp(-\Lambda')}{\Lambda'} \tag{46}$$

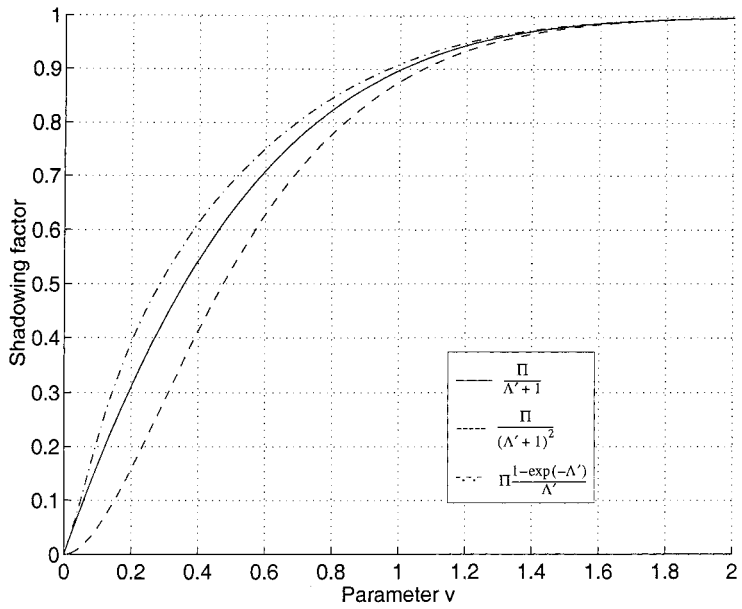

Figure 11. Comparison of the shadowing factors versus $v = \cot\theta/(\sigma_x\sqrt{2})$ for a monostatic configuration.

where Π is given by (21). Bourlier *et al* [15] showed that the Smith shadowing function is more accurate than Wagner's one which overestimates the shadow. Comparing (46) with (38) or (44), we can note that the shadowing factor should be $\Pi(v, v_s)/(\Lambda' + 1)^2$ instead of $\Pi(v, v_s)/(\Lambda' + 1)$, which involves an overestimation of the shadow, as shown in figure 11 for a monostatic configuration ($\Lambda = \Lambda'$ (13*a*) and $\Pi(v, v_s) = \Pi(v)$ (21)). Thorsos [7] showed with the Wagner shadowing function that the results calculated with the stationary phase approximation are overestimated compared with those obtained from the integral equation. We can explain this by the fact that the shadowing function which is used overestimates the shadow and the square of the denominator is ignored. In a subsequent paper, we will compare our model with Thorsos's data [7].

The surface is assumed to be isotropic. With the same reasoning, the next subsection studies the scattering coefficient by considering a two-dimensional surface.

4.4. Two-dimensional sea rough surfaces

This subsection presents the incoherent scattering coefficient obtained from an anisotropic rough surface which obeys to a general representation of ocean-like autocorrelation given by (26*a*).

From (33) and (34), when the shadowing function is included, the integration over the azimuthal direction Φ cannot be determined analytically. This means that the incoherent component $\{\sigma_{pqI}^{SP}, \sigma_{pqI}^{SA}\}$ requires three integrations over $\{Z, \Phi, r\}$. If the statistical shadowing function is assumed to be independent of the unshadowed scattering coefficient, then the surface height joint characteristic function is given by (20).

Using the stationary phase method from (33), and making the variable transformation $u = r/L_c$, we obtain

$$\sigma_{INI}^{SP} = \frac{\Pi |q^2 U'_{pq}|^2 L_c^2}{4\pi q_z^2 (\Lambda' + 1)^2} \exp(-q_z^2 \omega^2) \int_0^\infty u \, \mathrm{d}u \left\{ \int_0^{2\pi} \exp\left[\mathrm{j} u L_c \sqrt{q_x^2 + q_y^2} \cos(\Phi - \varphi) \right] \right.$$
$$\left. \times (\exp\{q_z^2 \omega^2 [f_{00}(u) - \cos(2\Phi) f_{02}(u)]\} - 1) \, \mathrm{d}\Phi \right\}. \tag{47}$$

The use of (C4) leads to

$$\sigma_{INI}^{SP} = \frac{\Pi |q^2 U'_{pq}|^2 L_c^2}{q_z^2 (\Lambda' + 1)^2} \exp(-q_z^2 \omega^2) \int_0^\infty u \{\exp[q_z^2 \omega^2 f_{00}(u)] - 1\}$$
$$\times \left[J_0(a) I_0(b) + 2 \sum_{n=1}^{\infty} \cos(2n\phi) J_{2n}(a) I_n(b) \right] \mathrm{d}u \tag{48}$$

with

$$a = u L_c \sqrt{q_x^2 + q_y^2} \qquad b = q_z^2 \omega^2 f_{02}(u) \qquad \phi = a \tan(q_y / q_x). \tag{48a}$$

and $\{J_n, I_n\}$ are the nth-order Bessel functions of first and second kinds, respectively.

If the transmitter and receiver are in the same plane ($\varphi_s = \varphi$), then $\phi = \varphi$ which denotes the azimuthal direction with respect to the wind direction.

To illustrate the two-dimensional case, the model is applied to the sea surface by using a two-scale model. Therefore, the surface height is obtained by superposing both surfaces. The small scale which characterizes the capillary waves and the scattering coefficient are evaluated with, for example, the small-perturbation method. The high scale corresponding to the gravity waves and the scattering coefficient simulated in this subsection are computed with the stationary phase. Assuming that both of these scales are independent, the bistatic cross section is then evaluated from summing both of these terms.

From Elfouhaily *et al*'s [20] spectrum, Bourlier *et al* [19] modelled the two-dimensional sea surface height autocorrelation function expressed as

$$R_0(r, \Phi) = \omega^2 \left[\frac{\cos(r/L'_c)}{1 + (r/L_c)^2} - A \cos(2\Phi) \frac{J_2(r/L'_2)}{1 + (r/L_2)^2} \right] \tag{49}$$

with

$$\begin{array}{lll} \omega^2 = 3.953 \times 10^{-5} u_{10}^{4.04} & L_c = 0.154 u_{10}^{2.04} & L'_c = 0.244 u_{10}^{1.91} \\ A = 3.439 u_{10}^{0.11} & L_2 = 0.157 u_{10}^{1.95} & L'_2 = 0.138 u_{10}^{2.05} \end{array} \tag{49a}$$

where u_{10} is the wind speed at ten meters above the sea, and the parameters $\{\alpha, \beta\}$ are given by

$$\alpha = \omega^2 \left(\frac{2}{L_c^2} + \frac{1}{L_c'^2} \right) \qquad \beta = \frac{\omega^2 A}{4 L_2'^2}. \tag{50}$$

Figure 12 represents the normalized bistatic incoherent scattering coefficient σ_{INI}^{SP} (48) and σ_{USI}^{SP} (σ_{INI}^{SP} with $\{\Pi = 1, \Lambda' = 0\}$), for a two-dimensional sea surface versus the scattering angle. The wind directions are $\phi = \{0, 45, 90\}^\circ$, and different sea states $u_{10} = \{5, 10\}$ m s^{-1} are examined. The normalization is obtained from the maximum computed with $\phi = 90^\circ$. The electromagnetic wavelength is equal to $\lambda = 3$ cm characterizing a radar in the X-band ($f = 10$ GHz). The surface relative complex permittivity is equal to $56 - 38\mathrm{j}$ [26]

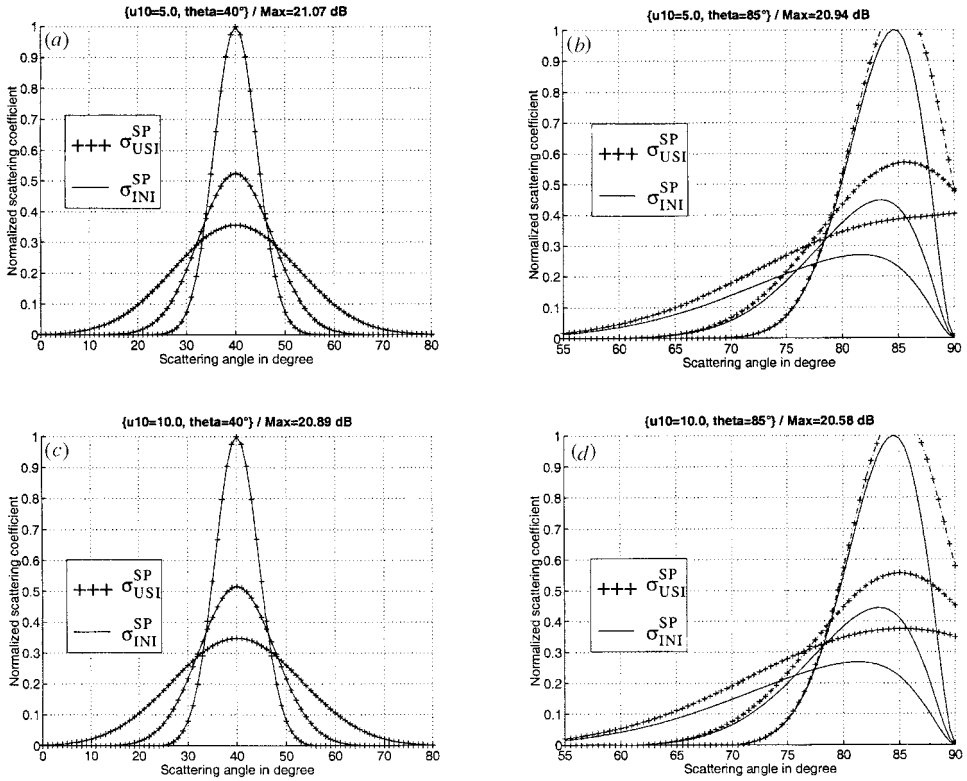

Figure 12. Normalized bistatic incoherent scattering coefficient $\sigma_{INI}^{SP}, \sigma_{USI}^{SP}$, for a two-dimensional sea surface versus the scattering angle with wind directions $\phi = \{0, 45, 90\}^\circ$. (*a*) $\{u_{10} = 5\ \mathrm{m\ s^{-1}}, |\theta| = 40^\circ\}$, (*b*) $\{u_{10} = 5\ \mathrm{m\ s^{-1}}, |\theta| = 85^\circ\}$, (*c*) $\{u_{10} = 10\ \mathrm{m\ s^{-1}}, |\theta| = 40^\circ\}$ and (*d*) $\{u_{10} = 10\ \mathrm{m\ s^{-1}}, |\theta| = 85^\circ\}$. The normalization is obtained from the maximum computed with $\phi = 90^\circ$.

corresponding to a temperature and salinity of the sea surface of 20 °C and 35 g $\mathrm{l^{-1}}$, respectively, with $\lambda = 3$ cm.

In figures 12(*a*) and (*b*), the wind speed $u_{10} = 5\ \mathrm{m\ s^{-1}}$ involves the surface RMS slopes $\sigma_X = \{0.0775, 0.0638, 0.0462\}$ with respect to $\phi = \{0, 45, 90\}^\circ$, $\omega = 0.162$ m, $k\omega = 34.00$ and $|\theta| = \{40, 85\}^\circ$. As ϕ increases, the surface slope variance decreases involving the bandwidth decreasing, whereas the maximum enhances. For near-grazing incidence angle, we see that the shadowing effect is not negligible.

In figures 12(*c*) and (*d*), the parameters are the same as in figures 12(*a*) and (*b*), respectively, with $u_{10} = 10\ \mathrm{m\ s^{-1}}$. This means that $\sigma_X = \{0.0784, 0.0644, 0.0463\}$, $\omega = 0.658$ m, $k\omega = 137.89$. Although $k\omega$ is greater than in figures 12(*a*) and (*b*), the behaviour is similar to a weak diminution of the maximum because the slope variance is greater. This fact comes from the fact that $k\omega$ is so large that the geometrical optics approximation is valid, and the scattering coefficient then becomes independent of $k\omega$ (see (39) for an isotropic surface).

In figure 13, for a two-dimensional sea surface, the bistatic incoherent scattering coefficient σ_{INI}^{SP} is represented versus the scattering angle with $\{\phi = 0^\circ, u_{10} = 10\ \mathrm{m\ s^{-1}}, |\theta| = 80^\circ\}$ according to the frequency $f = \{1, 5, 10\}$ GHz and the polarizations $\{VV, HH\}$. Since

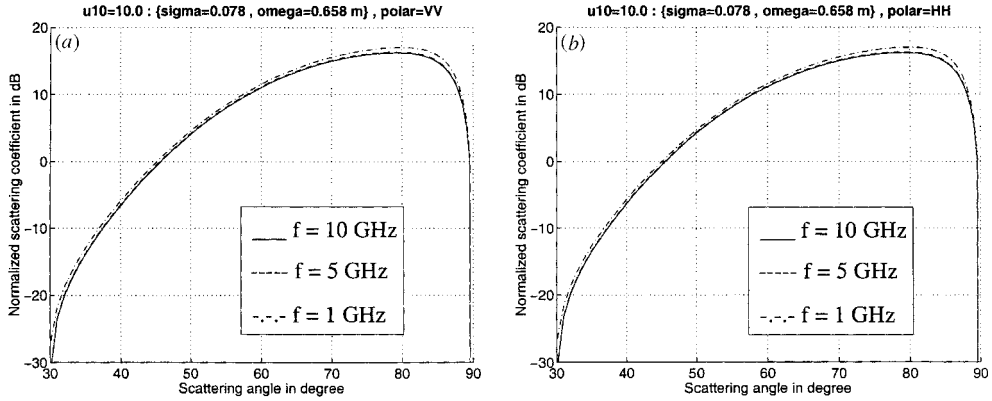

Figure 13. Bistatic incoherent scattering coefficient σ_{INI}^{SP} for a two-dimensional sea surface versus the scattering angle with $\{\phi = 0^\circ, u_{10} = 10 \text{ m s}^{-1}, |\theta| = 80^\circ\}$ and according to the polarizations: (a) VV, (b) HH. $f = 10$ GHz (full curve), $f = 5$ GHz (broken curve) and $f = 1$ GHz (chain curve).

the sea surface is a dispersive medium, its permittivity depends on the frequency. With a temperature and salinity of the sea surface of 20 °C and 35 g l^{-1}, we have from [26] $\varepsilon_r(f = \{1, 5, 10\} \text{ GHz}) = \{72 - 85\text{j}, 67 - 41\text{j}, 56 - 38\text{j}\}$. As depicted in figure 12, the maximum of the scattering coefficient decreases when $k\omega$ proportional to the wind speed u_{10} increases. Therefore, in figure 13, since $k\omega = 2\pi c/f = \{137.89, 68.94, 13.79\}$ the incoherent component should increase with the frequency f. However, the sea permittivity decreases with frequency involving as the Fresnel coefficients in $\{VV, HH\}$ polarizations increase when the frequency decreases. Both of these phenomena are then in opposition and allow us to explain that the scattering coefficient observed in figure 13 increases when the frequency decreases. We can also note that the scattering coefficient varies weakly with the polarization.

No comparison with experimental data is made, because it is very difficult to find measurements in the literature according to the wind direction (i.e. for an anisotropic surface) and in the scattering case. Moreover, as shown by Bourlier *et al* [12], in the one-dimensional backscattering case the shadowing effect can be neglected, involving our model becoming similar to the classical stationary phase method without a shadowing effect.

5. Conclusion

The stationary phase and the scalar approximation [1] applied to scattering from one- and two-dimensional rough surfaces with a shadowing effect have been examined. These solutions are obtained from the Kirchhoff integral which assumes that both the surface RMS radius of curvature R_c and the surface length correlation L_c are much greater than the wavelength. For the first assumption, we can also quote $k R_c \cos^3(\theta) > 1$ [3,7], where θ is the incidence angle. R_c can be evaluated [21,22] from the joint probability density (PDF). From the stationary phase method, the scattering coefficient is then derived as a function of the geometrical problem, the Fresnel coefficients and the surface height joint characteristic function, giving the surface random behaviour. With the scalar approximation, the radar bistatic cross section depends on the previous characteristic function and on the expected values, which characterize the integration over the slopes.

The statistical dependence of the shadowing function over the characteristic function is studied. This means that the surface height density probability, assumed to be Gaussian, is modified by the shadow and loses its Gaussian behaviour (figure 2). With the Smith shadowing function, figure 3 shows that the characteristic function obtained from the shadowing function independence, is greater than that computed with the statistical dependence. Consequently, the characteristic function is overestimated.

The simulations show that the shadowing effect is important at near-grazing incidence and scattering angles and when the surface slope variance becomes large. From an isotropic perfectly-conducting surface, our models are compared with experimental data (see figures 5–8 in O'Donnell and Mendez [18]). According to the scattering angle, our results deviate from the experimental data when the scattering angles are smaller than the specular direction. Above the specular direction, the shadowing effect involves a non-symmetrical behaviour and the models deviate less than those obtained without shadow. Although the shadowing function is included, this deviation may be explained due to the fact that the criterion $kR_c\cos^3(\theta) > 1$ is not verified for grazing incidence angles. The results computed from the scalar approximation are weakly smaller than those determined with the stationary phase.

From the two-scale model and the surface height autocorrelation expressed in [19], the incoherent scattering coefficient computed from the stationary phase method is applied to the sea surface for a given wavelength, with different sea states, according to the azimuthal wind direction.

Appendix A. Ensemble average with shadow

This appendix determines the ensemble average $\langle\cdots\rangle_{SA}$ (24) with shadow referred to as $\langle\cdots\rangle_{SA}^{S}$. When the shadowing effect is ignored, the integration ranges over the slopes are $]-\infty;\infty[$. From (17) and according to the location of the receiver, the shadowing effect within Υ' carries a restriction over the slopes $\{\gamma_X, \gamma_X'\}$ which is

$$\gamma_X \in [-\mu_m;\mu_p] \qquad \gamma_X' \in [-\mu_m;\mu_p] \qquad \text{with} \quad \mu_m \geqslant 0 \quad \mu_p \geqslant 0 \tag{A1}$$

and

$$\begin{aligned}
&\text{if} \quad \theta_s|\theta| \geqslant 0 \qquad \text{then} \quad \Upsilon(\mu+\gamma_X)\Upsilon(\mu_s-\gamma_X) \quad \Rightarrow \quad \{\mu_m=\mu,\mu_p=\mu_s\}\\
&\text{if} \quad |\theta_s| \leqslant |\theta| \qquad \text{then} \quad \Upsilon(\mu_s+\gamma_X) \quad \Rightarrow \quad \{\mu_m=\infty,\mu_p=\mu_s\}\\
&\text{if} \quad |\theta| < |\theta_s| \qquad \text{then} \quad \Upsilon(\mu+\gamma_X) \quad \Rightarrow \quad \{\mu_m=\infty,\mu_p=\mu\}
\end{aligned} \tag{A2}$$

whereas the integration ranges over $\{\gamma_Y, \gamma_Y'\}$ remain $]-\infty;\infty[$. Using the new integration ranges over the slopes, the expected value with shadow E_{S4} becomes from (25)

$$E_{S4}(\cdots) = \int_{-\mu_m}^{\mu_p} \mathrm{d}\gamma_X \int_{-\mu_m}^{\mu_p} \mathrm{d}\gamma_X' \int_{-\infty}^{\infty} \mathrm{d}\gamma_Y \int_{-\infty}^{\infty} \mathrm{d}\gamma_Y'(\cdots)p(\vec{V}_{XY}). \tag{A3}$$

Neglecting the correlation between the slopes and heights, we obtain

$$E_{S4}(\cdots) = p_S(z',z'')\int_{-\mu_m}^{\mu_p} \mathrm{d}\gamma_X \int_{-\mu_m}^{\mu_p} \mathrm{d}\gamma_X' \int_{-\infty}^{\infty} \mathrm{d}\gamma_Y \int_{-\infty}^{\infty} \mathrm{d}\gamma_Y'(\cdots)p(\gamma_X,\gamma_X',\gamma_Y,\gamma_Y'). \tag{A4}$$

where $p_S(z',z'')$ is the surface height joint probability density with shadow defined by (C3) of [12]. The derivation of the ensemble average requires knowledge of $E_{S4}(1)$, $E_{S4}(\gamma_X)$, $E_{S4}(\gamma_X')$, $E_{S4}(\gamma_Y)$ and $E_{S4}(\gamma_Y')$.

$E_{S4}(1)$ is given by

$$E_{S4}(1) = p_S(z',z'')\int_{-\mu_m}^{\mu_p} \mathrm{d}\gamma_X \int_{-\mu_m}^{\mu_p} \mathrm{d}\gamma_X' \left[\int_{-\infty}^{\infty}\int_{-\infty}^{\infty} p(\gamma_X,\gamma_X',\gamma_Y,\gamma_Y')\,\mathrm{d}\gamma_Y\,\mathrm{d}\gamma_Y'\right]. \tag{A5}$$

The term between brackets is equal to the surface slope joint probability density $p(\gamma_X, \gamma'_X)$ given by

$$p(\gamma_X, \gamma'_X) = \frac{1}{2\pi\sigma_X^2(1-f_2^2)^{1/2}} \exp\left[-\frac{1}{2\sigma_X^2(1-f_2^2)}(\gamma_X^2 + \gamma_X^{2\prime} - 2f_2\gamma_X\gamma'_X)\right] \tag{A6}$$

with

$$f_2 = -R_2/\sigma_X^2 \qquad \text{and} \qquad R_2 = \mathrm{d}^2R_0/\mathrm{d}r^2 \tag{A7}$$

which corresponds to the minus surface slope two-dimensional autocorrelation function. The following variable transformations

$$\begin{aligned} \gamma_X &= \sigma_X[X(1+f_2)^{1/2} - X'(1-f_2)^{1/2}] \\ \gamma'_X &= \sigma_X[X(1+f_2)^{1/2} + X'(1-f_2)^{1/2}] \end{aligned} \tag{A8}$$

lead in (A5) to

$$E_{S4}(1) = \frac{p_S(z', z'')}{\pi} \int_{-X_p}^{X_p} \mathrm{d}X \int_{-X'_m}^{X'_p} \exp(-X'^2 - X^2)\,\mathrm{d}X' \tag{A9}$$

with

$$X'_m = \frac{\mu_m}{\sigma_X(1-f_2)^{1/2}} \qquad X'_p = \frac{\mu_p}{\sigma_X(1-f_2)^{1/2}} \qquad X_p = \frac{\mu_m + \mu_p}{2\sigma_X(1+f_2)^{1/2}}. \tag{A10}$$

Performing the integrations over $\{X, X'\}$, we obtain

$$E_{S4}(1) = \frac{p_S(z', z'')}{2}[\mathrm{erf}(X'_p) + \mathrm{erf}(X'_m)]\,\mathrm{erf}(X_p) \tag{A11}$$

where erf is the error function.

The expected value of $E_{S4}(\gamma_X)$ is expressed as

$$E_{S4}(\gamma_X) = \int_{-\mu_m}^{\mu_p} \int_{-\mu_m}^{\mu_p} \gamma_X\, p(\gamma_X, \gamma'_X)\,\mathrm{d}\gamma_X\,\mathrm{d}\gamma'_X. \tag{A12}$$

Using (A8) variable transformations and performing the integrations over $\{X, X'\}$, we show that

$$E_{S4}(\gamma_X) = -p_S(z', z'')\frac{\sigma_X(1-f_2)^{1/2}}{2\sqrt{\pi}}\left[\exp(-X_p'^2) - \exp(-X_m'^2)\right]\mathrm{erf}(X_p). \tag{A13}$$

Applying the same method as previously, the expected value of $E_{S4}(\gamma'_X)$ is given by

$$E_{S4}(\gamma'_X) = -E_{S4}(\gamma_X). \tag{A14}$$

The expected value $E_{S4}(\gamma'_Y)$ is defined as follows:

$$E_{S4}(\gamma'_Y) = \int_{-\mu_m}^{\mu_p} \int_{-\mu_m}^{\mu_p} \mathrm{d}\gamma_X\,\mathrm{d}\gamma'_X \left[\int_{-\infty}^{\infty} \gamma'_Y\, p(\gamma_X, \gamma'_X, \gamma'_Y)\,\mathrm{d}\gamma'_Y\right]. \tag{A15}$$

From (D9) of [12], the integration over γ'_Y leads to

$$\begin{aligned} E_{S4}(\gamma'_Y) = \frac{p_S(z', z'')}{\sigma_X^2(1-f_2^2)} \int_{-\mu_m}^{\mu_p} \int_{-\mu_m}^{\mu_p} &\left[\gamma'_X(\sigma_{XY}^2 - \sigma_X\sigma_Y f_2 f_{36}) + \gamma_X(\sigma_X\sigma_Y f_{36} - \sigma_{XY}^2 f_2)\right] \\ &\times p(\gamma_X, \gamma'_X)\,\mathrm{d}\gamma_X\,\mathrm{d}\gamma'_X \\ = \frac{E(\gamma'_X)(\sigma_{XY}^2 - \sigma_X\sigma_Y f_2 f_{36}) + E(\gamma_X)(\sigma_X\sigma_Y f_{36} - \sigma_{XY}^2 f_2)}{\sigma_X^2(1-f_2^2)} \end{aligned} \tag{A16}$$

where

$$f_{36} = -C_{36}/(\sigma_X \sigma_Y) \qquad \text{with} \quad C_{36} = \frac{2\sin(2\Phi)(r R_{12} - R_{02})}{r^2}. \tag{A17}$$

From (A14) we obtain

$$E_{S4}(\gamma'_Y) = \frac{\sigma_X \sigma_Y f_{36} - \sigma_{XY}^2}{\sigma_X^2 (1 - f_2)} E(\gamma_X). \tag{A18}$$

Applying the same method as the derivation of $E_{S4}(\gamma'_Y)$, we can show that the expected value $E_{S4}(\gamma_Y)$ is computed from (A16) by swapping $\{\gamma_X, \gamma'_X\}$ in $\{\gamma'_X, \gamma_X\}$, respectively, and as $E_{S4}(\gamma'_X) = -E_{S4}(\gamma_X)$, we obtain

$$E_{S4}(\gamma_Y) = -E_{S4}(\gamma'_Y). \tag{A19}$$

From (24), the ensemble average with shadow can be expressed as

$$\langle \cdots \rangle_{SA}^{S} = \int_{-\infty}^{\infty} \int_{-\infty}^{\infty} \left[|a_0|^2 E_{S4}(1) + A_1 E_{S4}(\gamma_X) + A_1^* E_{S4}(\gamma'_X) + A_2 E_{S4}(\gamma_Y) + A_2^* E_{S4}(\gamma'_Y) \right] \times \exp[\mathrm{j} q_z (z' - z'')] \, \mathrm{d}z' \, \mathrm{d}z''. \tag{A20}$$

As $E_{S4}(\gamma_X) = -E_{S4}(\gamma'_X)$ and $E_{S4}(\gamma_Y) = -E_{S4}(\gamma'_Y)$, equation (A20) becomes

$$\langle \cdots \rangle_{SA}^{S} = \int_{-\infty}^{\infty} \int_{-\infty}^{\infty} \left\{ |a_0|^2 E_{S4}(1) + 2\mathrm{j}[\mathrm{Im}(A_1) E_{S4}(\gamma_X) + \mathrm{Im}(A_2) E_{S4}(\gamma_Y)] \right\} \times \exp[\mathrm{j} q_z (z' - z'')] \, \mathrm{d}z' \, \mathrm{d}z'' \tag{A21}$$

where Im denotes the imaginary part. The substitution of (A5), (A13) and (A18) into (A21) and the use of $\{A_1, A_2\}$ leads to

$$\langle \cdots \rangle_{SA}^{S} = [B_0 - \mathrm{j} B_c \cos(\varphi - \Phi) - \mathrm{j} B_s \sin(\varphi - \Phi)] \times \int_{-\infty}^{\infty} \int_{-\infty}^{\infty} p_S(z', z'') \exp[\mathrm{j} q_z (z' - z'')] \, \mathrm{d}z' \, \mathrm{d}z'' \tag{A22}$$

with

$$\begin{aligned} B_0 &= \frac{|a_0|^2}{2} \mathrm{erf}(X_p)[\mathrm{erf}(X'_p) + \mathrm{erf}(X'_m)] \\ B_c &= \mathrm{Im}(a a_0) \sigma_X \left(\frac{1 - f_2}{\pi} \right)^{1/2} \mathrm{erf}(X_p)[\exp(X'^2_p) - \exp(X'^2_m)] \\ B_s &= \frac{\mathrm{Im}(a a_0)(\sigma_X \sigma_Y f_{36} - \sigma_{XY}^2)}{\sigma_X [\pi (1 - f_2)]^{1/2}} \mathrm{erf}(X_p)[\exp(X'^2_p) - \exp(X'^2_m)]. \end{aligned} \tag{A23}$$

The double integral over the surface elevations is equal to the surface height joint probability density with shadow χ_{S1} given by (18). Therefore,

$$\langle \cdots \rangle_{SA}^{S} = [B_0 - \mathrm{j} B_c \cos(\varphi - \Phi) - \mathrm{j} B_s \sin(\varphi - \Phi)] \chi_{S1}. \tag{A24}$$

From (A2) the terms $\{B_0, B_c, B_s\}$ are expressed as

if $\theta_s |\theta| \geqslant 0$ then (A23)

if $|\theta_s| \leqslant |\theta|$ then

$$\begin{cases} B_0 = \dfrac{|a_0|^2}{2}[1 + \mathrm{erf}(X'_p)] \qquad X'_p = \dfrac{\mu_s}{\sigma_X (1 - f_2)^{1/2}} \\ B_c = \mathrm{Im}(a a_0) \sigma_X \left(\dfrac{1 - f_2}{\pi} \right)^{1/2} \exp(-X'^2_p) \\ B_s = \dfrac{\mathrm{Im}(a a_0)(\sigma_X \sigma_Y f_{36} - \sigma_{XY}^2)}{\sigma_X [\pi (1 - f_2)]^{1/2}} \exp(-X'^2_p) \end{cases} \tag{A25}$$

if $|\theta| < |\theta_s|$ then the case of $|\theta_s| \leqslant |\theta|$ with $\mu_s = \mu$.

If the shadowing effect is not taken into account, then $\langle\cdots\rangle_{SA}^{S} = |a_0|^2\chi_{S1}$ because the stationary Gaussian process is defined with zero mean, i.e. $E(\gamma_X) = E(\gamma_X') = E(\gamma_Y) = E(\gamma_Y') = 0$.

Appendix B. Integration over the angular direction Φ

We need to solve the following integral over Φ

$$I = \int_0^{2\pi} \exp[\mathrm{j}x\cos(\Phi-\varphi)]\cos[a(\Phi-\varphi)]\,\mathrm{d}\Phi \tag{B1}$$

where $a \geqslant 0$ is an integer. The complex exponential can be expressed as [27]

$$\exp[\mathrm{j}x\cos(\Phi-\varphi)] = J_0(x) + 2\sum_{m=1}^{\infty}\mathrm{j}^m J_m(x)\cos[m(\Phi-\varphi)] \tag{B2}$$

where J_m is the Bessel function of the first kind and order m. Substituting (B2) into (B1) we obtain

$$I = J_0(x)\int_0^{2\pi}\cos[a(\Phi-\varphi)]\,\mathrm{d}\Phi + 2\sum_{m=1}^{\infty}\mathrm{j}^m J_m(x)\int_0^{2\pi}\cos[m(\Phi-\varphi)]\cos[a(\Phi-\varphi)]\,\mathrm{d}\Phi. \tag{B3}$$

The integration over Φ gives

$$\int_0^{2\pi}\cos[a(\Phi-\varphi)]\,\mathrm{d}\Phi = \begin{cases} 2\pi & \text{if} \quad a = 0 \\ 0 & \text{otherwise} \end{cases} \tag{B4}$$

and

$$\begin{aligned}\int_0^{2\pi}\cos[m(\Phi-\varphi)]\cos[a(\Phi-\varphi)]\,\mathrm{d}\Phi &= \frac{1}{2(a-m)}\{\sin[2\pi(a-m) - a\varphi + m\phi] \\ &\quad + \sin[a\varphi - m\phi]\} + \frac{1}{2(a+m)}\{\sin[2\pi(a+m) + a\varphi - m\phi] + \sin[a\varphi + m\phi]\}.\end{aligned} \tag{B5}$$

Since $a+m$ is never equal to zero ($a \geqslant 0$, $m \geqslant 1$), the second term of this integral is zero, whereas the first term is different to zero for $a - m = 0$, and we have

$$\begin{aligned}&\int_0^{2\pi}\cos[m(\Phi-\varphi)]\cos[a(\Phi-\varphi)]\,\mathrm{d}\Phi \\ &\quad = \lim_{a\to m}\frac{\sin[\pi(a-m)]\cos[\pi(a-m) - a\varphi + m\phi]}{a-m} \\ &\quad = \begin{cases} \pi\cos[a(\phi-\varphi)] & \text{if} \quad a = m \\ 0 & \text{otherwise.} \end{cases}\end{aligned} \tag{B6}$$

Substituting (B6) and (B4) into (B3), we finally obtain

$$\int_0^{2\pi}\exp[\mathrm{j}x\cos(\Phi-\varphi)]\cos[a(\Phi-\varphi)]\,\mathrm{d}\Phi = 2\pi\mathrm{j}^a J_a(x)\cos[a(\Phi-\varphi)] \tag{B7}$$

with $a \geqslant 0$ and integer.

Appendix C. Angular integration for a two-dimensional surface

We need to solve the following integral over Φ:

$$C_0 = \int_0^{2\pi} \exp[\mathrm{j}a\cos(\Phi-\varphi) - b\cos(2\Phi)]\,\mathrm{d}\Phi. \tag{C1}$$

The complex exponential can be expressed as [27]

$$\begin{aligned} \exp[\mathrm{j}a\cos(\Phi-\varphi)] &= J_0(a) + 2\sum_{m=1}^{\infty} \mathrm{j}^m J_m(a)\cos[m(\Phi-\varphi)] \\ \exp[-b\cos(2\Phi)] &= J_0(\mathrm{j}b) + 2\sum_{n=1}^{\infty} \mathrm{j}^n J_n(\mathrm{j}b)\cos[2n\Phi] \end{aligned} \tag{C2}$$

where J_m is the Bessel function of the first kind and order m. Substituting (C2) into (C1) and performing the integration over Φ we show

$$C_0 = 2\pi\left\{J_0(a)J_0(by) + 2\sum_{m=1}^{\infty}\sum_{n=1}^{\infty}\delta(m-2n)\cos(2n\phi)J_m(a)J_n(jb)\mathrm{j}^{m+n}\right\} \tag{C3}$$

where δ is the Dirac function. Using the relation $J_n(\mathrm{j}b) = \mathrm{j}^n I_n(b)$, where I_n denotes the Bessel function of the second kind and order n, we obtain

$$C_0 = 2\pi\left\{J_0(a)I_0(b) + 2\sum_{n=1}^{\infty}\cos(2n\phi)J_{2n}(a)I_n(b)\right\}. \tag{C4}$$

References

[1] Ulaby F T, Moore R K and Fung A K 1982 *Microwave Remote Sensing* vol II (Reading, MA: Addison-Wesley)
[2] Ulaby F T and Elachi C 1990 *Radar Polarimetry for Geoscience Application* (Boston, MA: Artech House)
[3] Olgilvy J A 1991 *Theory of Wave Scattering from Random Rough Surfaces* (Bristol: Hilger)
[4] Beckmann P and Spizzichino A 1963 *The Scattering of Electromagnetic Waves from Rough Surfaces: Part I. Theory* (London: Pergamon)
[5] Voronovich A G 1994 *Wave Scattering from Rough Surfaces (Springer Series on Wave Phenomena)* (Berlin: Springer)
[6] Thorsos E I and Jackson D R 1991 Studies of scattering theory using numerical methods *Waves Random Media* **3** S165–90
[7] Thorsos E I 1988 The validity of the Kirchhoff approximation for rough surface scattering using a Gaussian roughness spectrum *J. Acoust. Soc. Am.* **83** 78–92
[8] Thorsos E I and Broschat S L 1989 The validity of the perturbation theory approximation for rough surface scattering using a Gaussian roughness spectrum *J. Acoust. Soc. Am.* **86** 261–77
[9] Thorsos E I and Broschat S L 1997 An investigation of the small slope approximation for scattering from rough surfaces. Part I. Theory *J. Acoust. Soc. Am.* **101** 2082–93
[10] Broschat S L and Thorsos E I 1997 An investigation of the small slope approximation for scattering from rough surfaces. Part II. Numerical studies *J. Acoust. Soc. Am.* **101** 2615–25
[11] Chevalier B and Berginc G 2000 Small slope approximation method: scattering of a vector wave from 2D dielectric and metallic surfaces with Gaussian and non-Gaussian statistics *SPIE Scattering Surface Roughness* **III** 22–32
[12] Bourlier C, Saillard J and Berginc G 2001 Theoretical study of the Kirchhoff integral from a two-dimensional randomly rough surface with shadowing effect: application to the backscattering coefficient for a perfectly-conducting surface *Waves Random Media* **11** 91–118
[13] Smith B G 1967 Lunar surface roughness, shadowing and thermal emission *J. Geophys. Res.* **72** 4059–67
[14] Smith B G 1967 Geometrical shadowing of a random rough surface *IEEE Trans. Antennas Propag.* **15** 668–71
[15] Bourlier C, Saillard J and Berginc G 2000 The shadowing function *Prog. Electromagn. Res.* **27** 225–87
[16] Wagner R J 1966 Shadowing of randomly rough surfaces *J. Opt. Soc. Am.* **41** 138–47

[17] Sancer M I 1969 Shadow-corrected electromagnetic scattering from a randomly rough surface *IEEE Trans. Antennas Propag.* **17** 577–85
[18] O'Donnell K A and Mendez E R 1987 Experimental study of scattering from characterized random surfaces *J. Opt. Soc. Am.* A **4** 1194–205
[19] Bourlier C, Saillard J and Berginc G 2000 Study of the sea behavior *Prog. Electromagn. Res.* **27** 193–225
[20] Elfouhaily T, Chapron B, Katsaros K and Vandemark D 1997 A unified directional spectrum for long and short wind-driven waves *J. Geophys. Res.* **102** 781–96
[21] Papa R J 1988 Conditions for the validity of physical optics in rough surface scattering *IEEE Trans. Antennas Propag.* **36** (5)
[22] Collaro A, Franceschetti G, Migliaccio M and Riccio D 1999 Gaussian rough surfaces and Kirchhoff approximation *IEEE Trans. Antennas Propag.* **47** (2)
[23] Bourlier C, Saillard J and Berginc G 2000 Effect of correlation between shadowing and shadowed points on the Wagner and Smith monostatic one-dimensional shadowing functions *IEEE Trans. Antennas Propag.* **48** 437–46
[24] Tsang L, Kong J and Shin R T 1985 *Theory of Microwave Remote Sensing (Wiley Series in Remote Sensing)* (New York: Wiley)
[25] Bahar E and Lee B S 1996 Radar scatter cross sections for two dimensional random rough surfaces—full wave solution and comparisons with experiments *Waves Random Media* **6** 1–23
[26] Daout F, Kenchaf A and Saillard J 1994 Effect of the salinity and temperature on the electromagnetic field scattered by the sea surface *Ocean's Symp. (Brest)* **1** 110–15
[27] Abramowitz M and Segun I A 1972 *Handbook of Mathematical Functions* (New York: Dover)